The low-temperature magnetic signature of Fe-rich serpentine in CM2 chondrites: Comparison with terrestrial cronstedtite and evolution with the degree of alteration

Agnès Elmaleh, Serena Chiara Tarantino, Michele Zema, Bertrand Devouard, Michel Fialin

Geochemistry Geophysics Geosystems G3

Article
Volume 13, Number 5
19 May 2012
Q05Z42, doi:10.1029/2011GC003964
ISSN: 1525-2027

Published by AGU and the Geochemical Society

The low-temperature magnetic signature of Fe-rich serpentine in CM2 chondrites: Comparison with terrestrial cronstedtite and evolution with the degree of alteration

Agnès Elmaleh
Institut de Minéralogie et de Physique des Milieux Condensés, UPMC/CNRS, 4 Place Jussieu, Case 115, F-75252 Paris CEDEX 5, France (agnes.elmaleh@impmc.upmc.fr)

Serena Chiara Tarantino and Michele Zema
Dipartimento di Scienze della Terra e dell'Ambiente, Università degli Studi di Pavia, via Ferrata 1, I-27100 Pavia, Italy (serenachiara.tarantino@unipv.it; michele.zema@unipv.it)

Bertrand Devouard
Laboratoire Magmas et Volcans, 6 rue Kessler, F-63038 Clermont-Ferrand, France (b.devouard@opgc.univ-bpclermont.fr)

Michel Fialin
CAMPARIS, 4 Place Jussieu, Case 115, F-75252 Paris CEDEX 05, France (michel.fialin@upmc.fr)

[1] We have studied the low temperature magnetic properties of one CI and five CM2 chondrites, well characterized in the literature, and of cronstedtite, the Fe end-member of the (Fe,Mg)-serpentine solid solution. Cronstedtite is highly anisotropic and its relaxation properties below ≈10 K suggest a glassy magnetic behavior. Frustration of the magnetic interactions in octahedral layers would account for the observed magnetic freezing, with a possible role of the random distribution of ferric iron in tetrahedral layers. Based on the comparison between powders and crystals characterized by SCXRD and EMPA, we show that grain size and substitution of octahedral Fe by Mg induce changes in the position of the low-*T* magnetic susceptibility peak. A low-*T* peak is also found in each of the CM2 chondrites, but not in the CI chondrite. It is interpreted as the signature of Fe-serpentines, which are considered by most authors to have mostly formed during asteroïdal aqueous alteration events. The low-*T* magnetic properties of the less altered meteorites compare well with those of cronstedtite, and the position of the susceptibility peak varies with the published degree of alteration. By comparing magnetic data on reference cronstedtite, magnetic and published mineralogical data on CM2 chondrites, we suggest that the evolution of the low-*T* magnetic signature of the latter reflects bulk changes in Fe-serpentines' chemical composition, rather than only mixing between Fe-rich and Mg-rich serpentines. This is analogous to previous observations on the changes in Fe incorporation to Mg-serpentines during progressive serpentinization of abyssal peridotites.

Components: 12,600 words, 11 figures, 4 tables.

Keywords: bulk magnetometry; crystal-chemistry of serpentines; spin glass behavior; asteroidal processes; hydrothermal alteration.

Index Terms: 1028 Geochemistry: Composition of meteorites (3662, 6240); 1540 Geomagnetism and Paleomagnetism: Rock and mineral magnetism; 3954 Mineral Physics: X-ray, neutron, and electron spectroscopy and diffraction.

Received 22 November 2011; **Revised** 4 April 2012; **Accepted** 10 April 2012; **Published** 19 May 2012.

Elmaleh, A., S. C. Tarantino, M. Zema, B. Devouard, and M. Fialin (2012), The low-temperature magnetic signature of Fe-rich serpentine in CM2 chondrites: Comparison with terrestrial cronstedtite and evolution with the degree of alteration, *Geochem. Geophys. Geosyst.*, *13*, Q05Z42, doi:10.1029/2011GC003964.

1. Introduction

[2] Carbonaceous chondrites of the CM and CI families are pristine samples of the early Solar System. However, despite their pristine chemical character, they contain abundant hydrated and hydroxylated minerals, testifying of an early action of water that likely occurred on their parent bodies, as reviewed by *Zolensky et al.* [2008], with a possible partial nebular heritage [*Metzler et al.*, 1992; *Lauretta et al.*, 2000]. Deciphering the conditions of aqueous alteration is essential for understanding the formation of small Solar System bodies that might have significantly contributed to the terrestrial water budget. Water bearing phases of CM and CI chondrites are predominated by sheet silicates. In CM2 chondrites, which form a large group with evolving mineralogy, although chlorite and smectite have been observed [*Zolensky et al.*, 1993], the hydroxylated phases are mostly 1:1 phyllosilicates of the serpentine family, according to TEM [*Tomeoka and Buseck*, 1985; *Zolensky et al.*, 1993] or X-ray diffraction (XRD) [*Howard et al.*, 2009] analyses. Among these minerals, Fe-rich serpentines close to the Fe end-member cronstedtite (±Mg, Al) are a major component [e.g., *Tomeoka and Buseck*, 1985; *Zolensky et al.*, 1993; *Howard et al.*, 2009]. These minerals can be found mostly in the matrix of the CM2 chondrites, where they are often concentrated in clumps of serpentine-tochilinite intergrowths (formerly called "Poorly Characterized Phases" giving rise to their denomination of PCP) [*Tomeoka and Buseck*, 1985]. The relative proportion of Mg-rich and Fe-rich serpentines varies among the meteorites, which has been interpreted by several authors as a marker of varying degrees of alteration [*Browning et al.*, 1996; *McSween*, 1979], with the possible influence of the initial anhydrous mineralogy [*Howard et al.*, 2009]. The aqueous alteration of CM asteroïdal parent bodies is in many ways comparable to the serpentinization of ultramafic rocks on Earth (initial ferromagnesian silicates assemblage, moderate temperature) [*Browning et al.*, 1996] although the initial chondritic material contains higher amounts of S and Fe. The partitioning of Fe among secondary phases in serpentinized peridotites is a good proxy for the degree of serpentinization [*Oufi and Cannat*, 2002]. Therefore, the Fe-serpentines mineralogy is an important proxy for better understanding the processes that have shaped CM2 parent bodies.

[3] Determining bulk serpentines mineralogy is made difficult by their complex crystal-chemistry. Moreover, Electron Microprobe Analyses (EMPA) of the matrix generally take into account several phyllosilicate grains and possibly other minerals such as sulfides because of the small size of the crystallites, as outlined by *Rubin et al.* [2007]. The use of several methods such as magnetism, together with IR spectroscopy [*Beck et al.*, 2010] or powder X-Ray Diffraction [*Howard et al.*, 2009] and direct TEM determination [*Zolensky et al.*, 1993; *Lauretta et al.*, 2000; *Zega and Buseck*, 2003] would help deciphering the bulk mineralogy of serpentines in CM2 chondrites. Magnetism is an important tool for studying the iron-rich mineralogy of meteorites [e.g., *Hyman and Rowe*, 1986; *Thorpe et al.*, 2002; *Kohout et al.*, 2007]. Room temperature magnetic and other physical properties (most notably χ, the magnetic susceptibility and the grain density) have been used for classifying carbonaceous meteorites [*Rochette et al.*, 2008]. At room temperature, the magnetic properties of non-ordinary chondrites are predominated by the presence of magnetite, Fe,Ni-alloys and iron sulfides [*Rochette et al.*, 2008]. Iron-rich phyllosilicates are paramagnetic at RT, but they show various patterns of magnetic ordering at low temperature, giving rise to magnetic susceptibility peaks below 60 K (T_p) [*Coey et al.*, 1981, 1982, 1989; *Rancourt et al.*, 1994]. Hence, these phases cannot play any role in planetary field recording, but their magnetic properties should be useful for deciphering their mineralogy, which encloses key information about the conditions of formation of carbonaceous chondrites. The magnetic signature of the Fe-serpentines close to the cronstedtite end-member needs first to be assessed. In previous studies of cronstedtite, *Coey et al.* [1981, 1989] proposed an antiferromagnetic structure, with identical magnetic and structural cells, that would be quite different from those usually found in ferrous layer silicates with antiferromagnetically ordered sheets (e.g., greenalite [*Coey et al.*, 1981]), due to the high amounts of ferric iron in tetrahedral sites. Uncertainties remain, such as the position of the magnetic susceptibility peak and the possible evolution of the magnetic properties with the crystal-chemistry of the mineral. In this study of the low-*T*

magnetic properties of cronstedtite, we show evidence for a glassy magnetic behavior of the system. We then apply the observations made on powders and on structurally and chemically characterized single-crystals to the interpretation of the low-T magnetic properties of CM2 chondrites and their bearing to the degree of alteration of the meteorites.

2. Samples

2.1. Cronstedtite

[4] This mineral is formulated:

$$(Fe^{2+}_{3-x}Fe^{3+}_{x})(Si_{2-x}Fe^{3+}_{x})O_5(OH)_4.$$

The parameter x falls into the interval [0.5;≈0.8] in terrestrial crystals [*Kogure et al.*, 2002]. The structure of cronstedtite consists in the stacking of sheets built from a layer of (Fe^{3+}, Si)O_4 tetrahedra and a layer of (Fe^{2+}, Fe^{3+})$O_2(OH)_4$ octahedra. The crystal growth of terrestrial cronstedtite along the **c**-axis can be unusually large for a 1:1 trioctahedral phyllosilicate, giving rise to millimeter size single crystals, which have been used for obtaining oriented magnetic measurements. The specimens consist of jet-black crystals and come from the mineralogical collections of IMPMC (Paris) and LMV (Clermont-Ferrand). They were taken from the mines of Salsigne (France), Kisbanya (also called Herja, Rumania) and Przibram (Czech Republic). Samples from the latter two sites were studied previously by Single Crystal X-Ray Diffraction (SCXRD) [*Hybler et al.*, 2000, 2002], whereas cronstedtite from Salsigne has not been described so far. For each site, the various sub-samples, either crystals or powder made of hand-picked crystals, come from a single, multicentimeter size sample.

2.2. Chondrites

[5] We studied two fragments of 0.6–7.5 mg of five CM2 (Cold Bokkeveld, Mighei, Murchison, Murray and Nogoya) and one CI (Orgueil) chondritic falls from the Museum National d'Histoire Naturelle (MNHN), Paris. The CM2 were chosen for their varying degree of alteration according to the study of *Browning et al.* [1996].

3. Methods

3.1. Electron Microprobe Analysis of Cronstedtite Samples

[6] For each of the 3 mines samples, EMP analyses were performed on at least 5 hand picked tabular crystals including the ones measured by SCXRD and magnetometry. Crystals were mounted and measured on (001) cleavage surfaces. We used a CAMECA SX100 microprobe at CAMPARIS, with an operating tension of 15 kV, a current intensity of 10 nA and acquisition times of 50 ms. Matrix corrections were performed using the *Pouchou and Pichoir* [1985] (PAP) method. The sum of the oxides wt% obtained (MgO, SiO_2, Al_2O_3, CaO, MnO and FeO) is consistently lesser than 90% (Table 1), which can be explained both by the high hydroxyl content of the minerals and by the fact that part of the iron is present as Fe^{3+}. A correction was applied to the data, based on the calculation of the ferric iron content so that, according to the formula given in introduction, full occupancy of tetrahedral sites (number of Fe atoms + number of Si atoms in tetrahedral site=2) and octahedral sites (total number of cations=5) are granted, in the respect of electrical neutrality. Doing so, the number of equations exceeds the number of unknowns. There is a <1% difference between the calculated number of ferric iron in octahedral and tetrahedral positions (Table 1), in good agreement with the ideal formula. The recalculated iron oxides composition for each sample yields total oxides content of ≈87 to 88 wt%. The water contents evaluated using the structural formula are equal to ≈9 to 10 wt%. The calculated totals yield water contents lagging by up to 2–3 wt% from the theoretical values, at 2σ error. We checked that this lag did not affect the structural formula determinations of the latter by comparing the calculated totals with ratios of measured oxides. For instance, we found no correlation ($R^2 < 0.4$) with the FeO/SiO_2 content of individual measurements for each crystal.

3.2. Single Crystal X-Ray Diffraction of Cronstedtite Crystals

[7] SCXRD experiments were carried out on most of the crystals used for the magnetic measurements, in order to orient the crystals, check for polytype, degree of (dis)order, and crystal quality. Unfortunately, Salsigne crystal 1 was damaged following recovery after magnetic measurements. Salsigne crystal 2 was cut into halves along the (001) cleavage plane, and the one measured by SCXRD is called crystal 2bis in Figure 1 and Table 2. In Table 1, results from the two halves of the crystal are not distinguished as they yield statistically identical results. SCXRD analyses were conducted at RT using a Bruker AXS SMART-APEX diffractometer equipped with a CCD detector (resolution 512 × 512 pixels) and graphite-monochromatized Mo-Kα radiation (λ = 0.71073 Å).

Table 1. Chemical Composition of Terrestrial Cronstedtite Samples From EMPA

	Salsigne Mine						Przibram Mine						Kisbanya Mine			
	Mine Mean		Crystal 1		Crystal 2 and 2bis		Mine Mean		Crystal 1		Crystal 2		Mine Mean		Crystal 1	
	Mean wt%	S.D.	Mean wt%	S.D.	Mean wt%	S.D.	Mean wt%	S.D.	Mean wt%	S.D.	Mean wt%	S.D.	Mean wt%	S.D.	Mean wt%	S.D.
Measured Oxide Composition																
N	8 (105)		21		69		5 (50)		21		20		5 (39)		16	
FeO	67.26	1.17	65.88	0.36	66.57	0.62	57.89	1.49	55.72	0.56	57.13	0.55	66.17	1.42	64.16	0.57
MgO	0.05	0.04	0.01	0.01	0.07	0.03	5.16	0.23	5.22	0.16	5.27	0.15	0.02	0.03	0.02	0.02
SiO_2	17.73	0.69	17.65	0.19	17.72	0.69	21.09	0.54	21.35	0.40	21.89	0.31	18.63	1.19	20.61	0.23
Al_2O_3	0.02	0.01	0.01	0.02	0.02	0.02	0.02	0.01	0.02	0.02	0.02	0.03	0.01	0.01	0.02	0.03
CaO	0.01	0.01	0.01	0.02	0.01	0.02	0.01	0.01	0.01	0.01	0.03	0.04	0.01	0.01	0.02	0.02
MnO	0.02	0.01	0.02	0.02	0.01	0.02	1.44	0.11	1.28	0.09	1.38	0.10	0.01	0.01	0.01	0.01
Tot. measured	85.09	1.04	83.59	0.42	84.38	0.76	86.25	0.70	83.60	0.76	85.73	0.49	84.86	1.09	84.85	0.54
Iron Valence Corrections[a]																
FeO	38.74	0.86	38.45	0.31	38.60	0.44	33.26	0.58	33.27	0.71	34.11	0.41	39.88	1.55	42.29	0.36
Fe_2O_3	31.72	1.84	30.49	0.42	31.08	0.81	27.38	1.94	24.95	0.81	25.59	0.79	29.21	2.83	24.31	0.76
Tot. calculated	88.26	1.12	86.64	0.43	87.50	0.74	88.36	1.36	86.10	0.77	88.29	0.53	87.79	1.14	87.28	0.59

	Salsigne Mine						Przibram Mine						Kisbanya Mine			
	Mine Mean		Crystal 1		Crystal 2 and 2bis		Mine Mean		Crystal 1		Crystal 2		Mine Mean		Crystal 1	
	Mean	S.D.	Mean	S.D.	Mean	S.D.	Mean	S.D.	Mean	S.D.	Mean	S.D.	Mean	S.D.	Mean	S.D.
Number of Cations per Formula Unit[a]																
Fe^{3+} IV	0.81	0.05	0.79	0.01	0.79	0.04	0.66	0.04	0.61	0.02	0.61	0.02	0.74	0.07	0.61	0.02
Fe^{3+} VI	0.81	0.05	0.79	0.01	0.80	0.04	0.66	0.04	0.61	0.02	0.61	0.02	0.74	0.07	0.62	0.02
Fe^{2+} VI	2.19	0.04	2.21	0.01	2.20	0.04	1.77	0.04	1.81	0.03	1.81	0.02	2.25	0.07	2.38	0.02
Mg	0.01	0.004	0.001	0.001	0.01	0.00	0.49	0.02	0.51	0.02	0.50	0.01	0.002	0.004	0.002	0.002
Si	1.20	0.04	1.21	0.01	1.20	0.04	1.34	0.04	1.39	0.02	1.39	0.02	1.26	0.07	1.39	0.02
Mn	0.001	0.001	0.001	0.001	0.00	0.001	0.08	0.01	0.07	0.01	0.07	0.01	0.00	0.001	0.001	0.02

[a]Calculated on the basis of full occupancy of tetrahedral and octahedral sites. Mn is assumed to be at valence II. Salsigne: crystal 2 and 2bis, 2 halves of the same crystals yield identical results at 2σ and were treated together. S.D.: standard deviation. N: number of measurements; sites means and standard deviations: calculated from mean oxides composition of each crystal (the first figure is the number of crystals; the total number of analyses involved is between parentheses).

A 0.8 mm collimated beam size was used. The Bruker SMART system of programs was used for preliminary crystal lattice determination and data collection. The Bruker program SAINT+ was used for data reduction, including intensity integration, background and Lorentz-polarization corrections. Final unit-cell parameters were obtained by the Bruker GLOBAL least squares orientation matrix refinement procedure. The semi-empirical absorption correction of *Blessing* [1995], based on the determination of transmission factors for equivalent reflections, was applied using the Bruker program SADABS [*Sheldrick*, 2004]. Simulated precession images were calculated along the main crystallographic directions by the Bruker program APEX2, and confirmed that all the analyzed crystals belong to the 1*T*-polytype, with stacking disorders. Crystal 2 from the Przibram mine appears to be fractured and constituted by two main individuals sharing **c*** and misaligned of ca. 2° in the *ab* plane. In this case, intensity integration was performed by using a box size that is large enough to include the contributions of both individuals. The presence of extra-reflections due to the $\lambda/2$ effect was also evident in all the crystals. Correction was applied [*Kirschbaum et al.*, 1997] after testing for half-wavelength contribution by integrating data using a supercell with doubled lattice parameters and obtaining *hkl* data sets with or without $\lambda/2$ correction: intensities of all reflections with at least one odd index were close to zero when corrected. Operating conditions and experimental details on data collections are reported in Table 2.

[8] Structure refinements were carried out in space group *P*31*m* by full-matrix least squares using

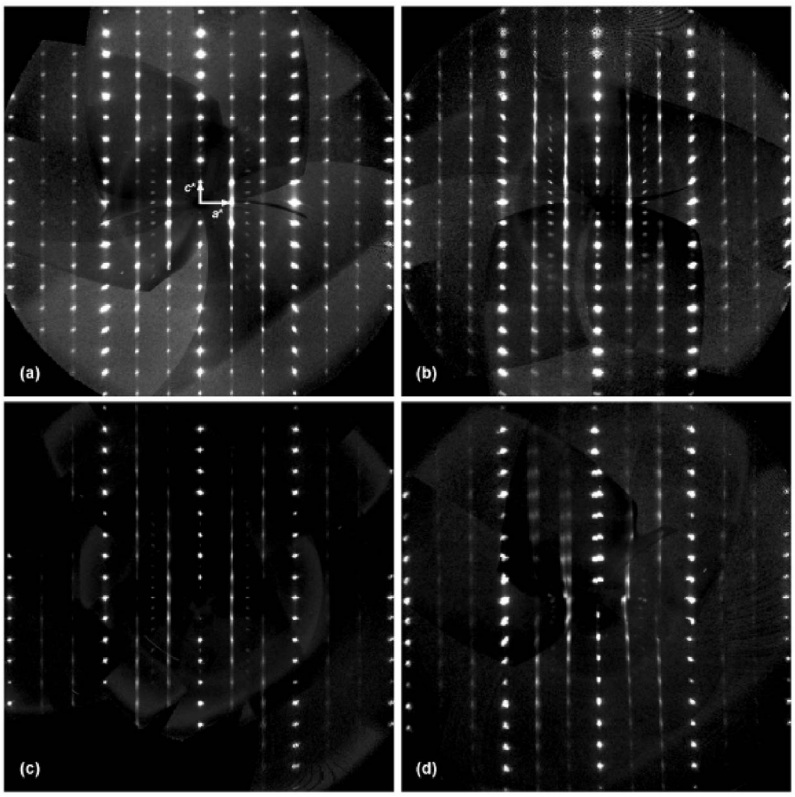

Figure 1. Calculated precession images of the *h*0*l* planes of cronstedtite-1*T* crystals. Vector **c*** is set vertically. (a) Kisbanya, crystal 1; (b) Salsigne, crystal 2bis; (c) Przibram, crystal 1; and (d) Przibram, crystal 2.

SHELXL-97 [*Sheldrick*, 1998]. Equivalent reflections were averaged and the resulting internal agreement factors R_{int} are reported in Table 2. The atomic scattering curves were taken from *Ibers and Hamilton* [1974]. For all the crystals, all non-hydrogen atoms were refined anisotropically. Structure factors were weighted according to $w = 1/[\sigma^2(F_o^2) + (AP)^2 + BP]$, where $P = (F_o^2 + 2\,F_c^2)/3$, and A and B were chosen for every crystal to produce a flat analysis of variance in terms of F_c^2 as suggested by the program. An extinction parameter x was refined to correct the structure factors according to the equation: $F_o = F_c\,k\,[1 + 0.001x\,F_c^2\,\lambda^3/\sin 2\theta]^{-1/4}$ (where k is the overall scale factor). All parameters were refined simultaneously. Refinements with scale factors of family and polytype reflections constrained to the same value (i.e., only one scale factor refined for all reflections) yield the appearance of ghost peaks in the difference-Fourier maps and failures in locating hydrogen atoms positions. Since precession images show diffuse streaking affecting the characteristic polytype diffractions, the Ďurovič effect [*Nespolo and Ferraris*, 2001] was taken into account in the final cycles of refinements and separate scale factors were set for the sub-family ($h - k = 3n$) and for the characteristic polytype reflections ($h - k \neq 3n$). This reduced sensibly the final *R*-factors, and made ghost peaks in the difference-Fourier maps to disappear. The hydrogen positions were then located in the difference-Fourier map and inserted in the refinement with isotropic displacement parameters. Isotropic displacement parameters of H1 atom were kept fixed at 1.2 times that of their neighbor oxygen atom for all the crystals. The values of the conventional agreement indices R_1 as well as the goodness of fit S are reported in Table 2. Fractional coordinates, anisotropic displacement parameters Uij and refined site occupancies at T1 sites are reported in Table S1 of the auxiliary material.[1] Observed and calculated structure factors are available from the authors.

3.3. Bulk Magnetometry

[9] Magnetic measurements were mostly performed using Quantum design Magnetic Properties

[1]Auxiliary materials are available in the HTML. doi:10.1029/2011GC003964.

Table 2. Single Crystal X-Ray Diffraction of Cronstedtite Crystals

	Kisbanya Crystal 1	Salsigne Crystal 2bis	Przibram Crystal 1	Przibram Crystal 2
		Data Collection		
Operating conditions	50 kV, 30 mA	50 kV, 25 mA	50 kV, 25 mA	40 kV, 20 mA
Scan mode	ω	ω	ω	ω
Scan width (°)	0.5	0.5	0.4	0.5
No. of goniometer settings	4	4	8	4
No. of frames collected	1440	1440	3600	1440
Exposure time (s/frame)	5	5	5	5
Detector-sample distance (cm)	5	5	10	5
2θ max (°)	62.26	61.70	65.70	64.50
		Unit Cell Parameters		
Space group	$P31m$	$P31m$	$P31m$	$P31m$
a (Å)	5.5078(5)	5.5000(5)	5.4689(6)	5.5012(5)
c (Å)	7.0989(7)	7.0920(6)	7.1172(9)	7.1602(6)
No. reflections for ucp	2510	1935	1283	1590
θ − range for ucp (°)	5.73–62.26	5.74–60.96	5.72–65.50	5.69–64.95
		Structure Refinement		
Reflections measured/unique	2817/441	2515/436	1966/502	3078/516
Average $I/\sigma(I)$	16.98	22.03	14.53	13.44
R_{int}[a] (%)	3.4	5.3	4.0	4.3
T_{min}/T_{max}	0.229	0.353	0.413	0.414
R_1[b] (%)	5.13	3.93	4.00	3.90
Reflections with $I > 2\sigma_I$	441	436	499	513
wR_2[b]	13.20	11.30	11.46	11.33
GOF[c]	1.172	1.141	1.132	1.148
BASF factor[d]	0.385	0.370	0.303	0.339
Max, min $\Delta\rho$ (e·Å^{-3})	1.41, −1.24	0.95, −1.38	2.12, −1.63	0.85, −1.17

[a] $R_{int} = \Sigma|F_o^2 - \langle F_o^2\rangle|/\Sigma F_o^2$.

[b] $R_1 = \Sigma||F_o| - |F_c||/\Sigma|F_o|$, calculated on reflections with $I > 2\sigma_I$; $wR_2 = [\Sigma[w(F_o^2 - F_c^2)^2]/\Sigma[w(F_o^2)^2]]^{1/2}$. R_{all} values are not reported since they coincide with R_1, being the intensities of almost all unique reflections $>2\sigma_I$.

[c] GOF = $[\Sigma\,[w(F_o^2 - F_c^2)^2]/(n-p)]^{0.5}$, where n is the number of reflections and p is the total number of parameters refined.

[d] BASF is the relative batch scale factor for non-family reflections. Such reflections are multiplied by this factor, as well as by the overall scale factor. Note that BASF is relative to F^2, while the overall scale factor is relative to F.

Measurement System instruments (MPMS) at the MPBT measurement platform of University Pierre et Marie Curie. For a few high field measurements (hysteresis at various T), we used a Vibrating Sample Magnetometer on a Physical Properties Measurement System (Groupe d'Etude de la Matière Condensée, Versailles). For some ac measurements (Kisbanya crystal 1, Przibram crystal 1, Salsigne crystal 2) and for the study of the decay of thermorement magnetization, which requires ultra-low remnant fields, we used the MPMS Evercool of the Institut de Physique du Globe de Paris. Powder samples of cronstedtite were contained in half a gel cap, over a length <4 mm. Measurements were performed either in a Zero Field Cooling (ZFC) mode, i.e., after cooling the sample from 300 K to 2 K prior to the application of the field, or in a Field Cooling mode (only for ZFC-FC dc magnetic susceptibility and viscosity measurements). The temperature was approached using the settle mode with a tolerance of ±0.05 K and temperature stability <1% at low temperatures. In dc mode, the applied field (**H**) was generally set to 10 mT, where a linear relation links the magnetization (M, Am^2/kg) to the applied field. Susceptibility data (χ, m^3/kg) are well modeled between 150 K and 300 K by the function:

$$\chi = \chi_0 + C/(T - \theta). \quad (1)$$

In this modified Curie-Weiss law, C is the Curie constant, θ, the Curie-Weiss temperature and χ_0 is the sum of all temperature-independent terms, estimated by extrapolating χ versus $1/T$ as $T \to \infty$. The effective moment per Fe ion, μ_{eff} expressed in Bohr magneton (μ_B), is deduced from C, the Curie constant:

$$\mu_{eff} = \left[(3.k_B.C.M)/\left(\mu_0.{\mu_B}^2.N_A.n_{Fe/molecule}\right)\right]^{1/2}. \quad (2)$$

In equation (2), k_B is the Boltzmann constant, μ_0, the permeability of free space, N_A, Avogadro's number, M the molar mass and $n_{Fe/molecule}$ the number of Fe atoms per unit formula, both deduced from EMPA. The dc mode was also used for hysteresis measurements up to 5 T. Magnets wound from superconducting wire trap remnant fields (up to a few mT) in their windings after being charged to high magnetic fields. The remnant fields, which do not have the same amplitude whether the applied field was positive or negative, induce slight shifts when the opening of the loop and the moments measured are weak, as it is often the case here. Moreover, once a persistent current is stored in the magnet, the magnetic field continues to relax, so that it is very difficult to quantify this effect.

[10] The ac mode was used to yield more accurate estimates of the low-field magnetic susceptibility peak position, and to study fast relaxation processes. Given the sensitivity of the system to low magnetic fields, dc viscosity measurements and ac measurements were performed using dc/ac applied fields ≤0.5 mT. The sensitivity of the MPMS theoretically allows one to measure moments of the order of 10^{-10} Am^2, but this limit is lowered for very small samples such as the millimeter size single crystals or the small meteorite fragments. For weakly magnetized samples, such as crystals along their hard axis, the ac signal or the remanent magnetization acquired in a low field were too weak to be measured accurately. The single crystals of cronstedtite have complex shapes (truncated pyramids or prisms, with nearly hexagonal, triangular or irregular shaped base), with variable aspect ratios, precluding accurate determinations of each demagnetizing factor N. The flattest sample, in which the largest shape anisotropy effects are expected, is Salsigne crystal 2. It has a rounded triangular base, and the demagnetizing factors for the field applied parallel or perpendicular to the **c**-axis were estimated by approximating the crystal shape by a cylinder, and using, for N, the magnetometric factors (suitable for SQUID measurements) calculated by *Chen et al.* [2006] and the relation linking the intrinsic volume magnetic susceptibility χ_i to the measured one (χ_{mes}): $1/\chi_i = 1/\chi_{mes} - N$. By taking two extreme cases - circumcircle and incircle cylinders - the maximum correction to be applied to the magnetic susceptibility along the **c**-axis is +1% ($N \approx 0.2$), and perpendicular to this axis, it is about +6% ($N \approx 0.6$). Using a MPMS, the uncertainty on the value of the measured field is of the order of 5% at low field, so that the demagnetizing field can be considered as small. When high fields are applied, the demagnetizing field is small with respect to the applied field.

4. Results

4.1. Characterization and Magnetic Properties of Terrestrial Cronstedtite

4.1.1. Chemical Composition

[11] The mean chemical composition of the cronstedtite samples is given in Table 1. Kisbanya and Salsigne mines samples are the closest to end-member cronstedtite, as they contain consistently ≤0.1 wt% impurities (oxides wt%). On the contrary, Przibram mine samples contain ≈6.5%, consisting of ≈5.2% MgO and ≈1.3% MnO. Calcium and aluminum were detected in some samples, but were not concentrated enough to be taken into account. Structural formulae for sites means, deduced from Table 1 are the following:

Salsigne (mean): $\left(Fe^{2+}_{2.19}Fe^{3+}_{0.81}\right)\left(Si_{1.20}Fe^{3+}_{0.81}\right)O_5(OH)_4$

Przibram (mean):

$\left(Fe^{2+}_{1.77}Mg_{0.49}Mn^{2+}_{0.08}Fe^{3+}_{0.66}\right)\left(Si_{1.34}Fe^{3+}_{0.66}\right)O_5(OH)_4$

Kisbanya (mean): $\left(Fe^{2+}_{2.25}Fe^{3+}_{0.74}\right)\left(Si_{1.26}Fe^{3+}_{0.74}\right)O_5(OH)_4$

4.1.2. Crystal Structures

[12] All the crystals studied by SCXRD belong to the 1*T* polytype (Table 2). The residuals obtained in structure refinements (3.90% to 5.13%) are particularly good despite the large sizes of the crystals (maximum dimensions about 1.5 mm), which should make them non-ideal material for this kind of analysis. Although one of them (Przibram crystal 2) appeared to be fractured, all crystals possess a well-defined **c**-axis. This allowed us to measure their magnetic properties with a field applied parallel or perpendicular to **c**. The 1*T* polytype, encountered in all the samples of this study, is the most common polytype in cronstedtite samples [*Bailey*, 1969]. In particular, *Hybler et al.* [2000] found this polytype to be predominant in samples from the Kisbanya mine. In Przibram mine, $2H_2$ polytypes were found to be predominant by *Hybler et al.* [2002], although the authors noticed polytypism within samples from this site. Concerning Salsigne, this is the first polytype determination.

[13] The degree of disorder is generally low, and the refined Batch Scale Factors (BASF, Table 2) only show relatively small differences among the

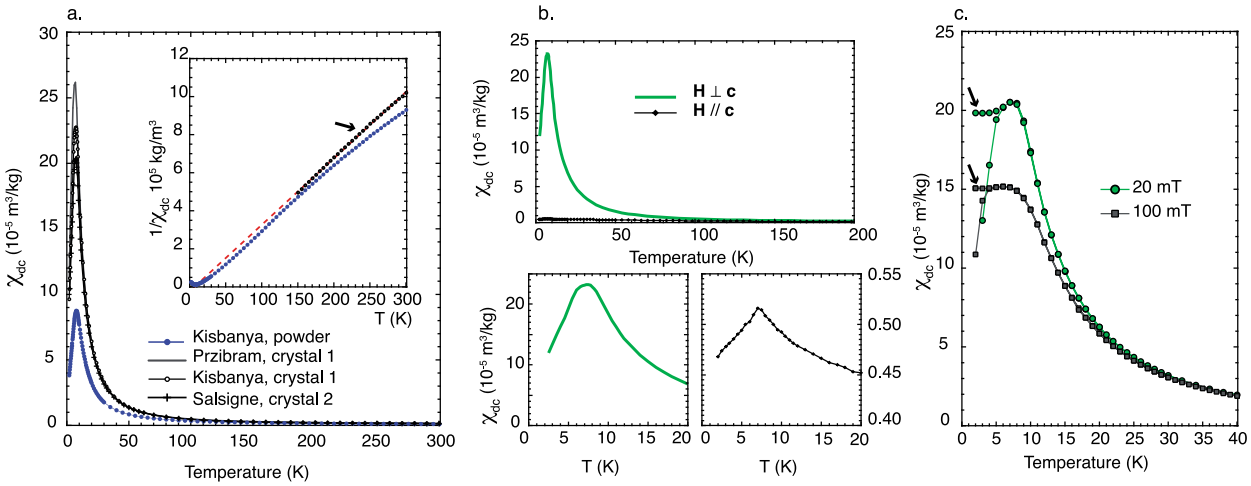

Figure 2. dc magnetic susceptibility measurements. (a) χ versus temperature ZFC curves (applied field: 10 mT) of a powder, and crystals of cronstedtite (**H** perpendicular to the **c**-axis). Inset shows $1/\chi$ data for Kisbanya powder; data corrected from a temperature independent term χ_0, and their fit to a straight line (dashed line) between 150 and 300 K are indicated by the arrow. (b) (top) Data from Salsigne crystal 2, obtained with the field applied along the **c**-axis, and perpendicular to the **c**-axis (applied field: 10 mT). (bottom) Zoom at low *T*. (c) ZFC-FC curves obtained for Salsigne crystal 1 (**H** perpendicular to **c**), with two different values of the applied field (20 and 100 mT). Below the maximum, the two curves split, and the FC curves (indicated by arrows) exhibit a plateau shape. Similar observations were made with **H** applied along **c**.

samples. However, both BASF values and the amount of diffuse streaks along the non-family lattice rows, as detected by the precession images, tend to suggest that Przibram crystals are slightly more disordered than the others, which show more spotty patterns (Figure 1). Przibram crystals show similar degrees of disorder concerning the sequence of layers in the structure (similar BASF values and diffuse streaking), but it must be pointed out that Przibram crystal 2 is fractured and constituted by two main individuals sharing **c*** and misaligned of ca. 2° in the *ab* plane.

4.1.3. Magnetic Properties

[14] A narrow peak is observed at low *T* in the ZFC susceptibility curves (Figure 2). Such a peak is a common feature of Fe-rich silicates, and in particular sheet silicates [*Coey et al.*, 1989, 1981, 1982; *Rancourt et al.*, 1994] regardless of the type of ordering [*Ballet et al.*, 1985]. The peak temperature is consistently <8.5 K in dc curves (Figure 2a). Literature data on Fe-rich serpentines indicate a well defined and broad peak at ≈9 K in berthierine, and a narrow peak at ≈17 K in greenalite [*Coey et al.*, 1981, Figure 4]. Two previous studies on cronstedtite report poorly defined peaks at $T < 10$ K [*Coey et al.*, 1981, Figure 4] (no peak is actually visible) and $T \approx 20$ K [*Coey et al.*, 1989] (no figure). We have no definite explanation for these discrepancies (sample heterogeneity for instance) but the measurements we made on a series of well-characterized crystals gave consistent results. The shape of the curves and the susceptibility values are markedly different whether the field is applied parallel or perpendicular to the **c**-axis, denoting a strong magnetic anisotropy (Figure 2b). Shape anisotropy should only make a small contribution, as deduced from worst case estimates of the demagnetizing factors (Methods). Crystal-field and spin-orbit coupling yield a strongly anisotropic ground state of Fe^{2+} in octahedral sites. In cronstedtite as in other phyllosilicates, the octahedra is flattened along the **c** direction [*Hybler et al.*, 2000, 2002]. This yields an effectively trigonal point symmetry around ferrous iron and provides for hard **c**-axis anisotropy in sheet silicates containing ferrous iron [*Ballet et al.*, 1985]. Peak temperatures obtained with the field applied parallel or perpendicular to **c** are, however, equivalent ±0.2 K (Figure 2b and Table 3).

[15] A progressive opening of the hysteresis loops is observed as *T* is lowered below ≈10 K. As shown in Figure 3, there is no hysteresis at 200 K. At 3 K, the lowest *T* used in this experiment, the opening is maximal, with highest coercive force (H_C) and remanence values (M_r) of ≈17 mT and 2 Am^2/kg, respectively. The decrease of M_r with *T* is abrupt: over 99% is lost between 3 K and 9 K when the

Table 3. Magnetic Properties of Cronstedtite Crystals and Powders

Samples	Susceptibility Measurements[a]					Hysteresis Measurements[f] (T = 4.2 K)		
	T_p dc[b] (K)	χpeak[b]	χ(2 K)[b]	χ(RT)[b]	T_p ac, K	M(5 T)	M_r	H_c
				Crystals				
Salsigne mine								
Crystal 1								
H // **c**	7.5 (±0.5)	1.3	0.8	0.1		38.18	0.18	8.5
H ⊥ **c**	7.75 (±0.5)	20.5	9.0	0.1	7.75 (±0.5)[c]	106.98	0.52	3.6
Crystal 2								
H // **c**	7.25 (±0.2)	0.5	0.5	0.1		19.60	0.06	13.6
H ⊥ **c**	7.4 (±0.2)	23.2	12.0[d]	0.1	7.75 (±0.2)	108.58	0.7	5.8
Kisbanya mine								
Crystal 1								
H // **c**	7.25 (±0.2)	0.9	0.6	0.1		27.24	0.09	11.0
H ⊥ **c**	7.4 (±0.2)	22.7	9.6	0.2	7.75 (±0.5)	110.92	0.52	3.3
Przibram mine								
Crystal 1								
H // **c**	6.75 (±0.3)	0.7	0.6	0.1		19.90	0.04	4.4
H ⊥ **c**	6.75 (±0.3)	26.2	11.0	0.2	7 (±0.2)	94.23	0.20	0.8
Crystal 2								
H // **c**	6.6 (±0.1)	3.2	1.4	0.1		15.49	0.03	6.9
H ⊥ **c**	6.7 (±0.1)	23.6	9.7	0.2	6.9 (±0.1)	96.56	0.20	1.6
				Powders				
Salsigne mine	7.9 (±0.2)	6.3	5.1	0.2	8.8 (±0.1)	61.38	0.42	7.1
Kisbanya mine[e]	7.8 (±0.2)	8.8	3.8	0.1	8.1 (±0.2)	64.86	0.78	12.5
Przibram mine	7.5 (±0.1)	6.7	2.6	0.1	7.8 (±0.1)	58.06	0.61	9.0

[a]Susceptibility: χ: in 10^{-5} m^3/kg; peak: at T_p: peak temperature. ac measurements: frequency: 10 Hz except as indicated.
[b]dc measurements obtained using an induction of 10 mT except Salsigne crystal 1: 20 mT.
[c]Frequency: 30 Hz.
[d]T = 2.5 K.
[e]Susceptibility and hysteresis results were obtained from two different powder samples.
[f]Hysteresis: M: magnetization at 5 T, Am^2/kg; M_r: remanence, same unit; H_c: coercive force, mT.

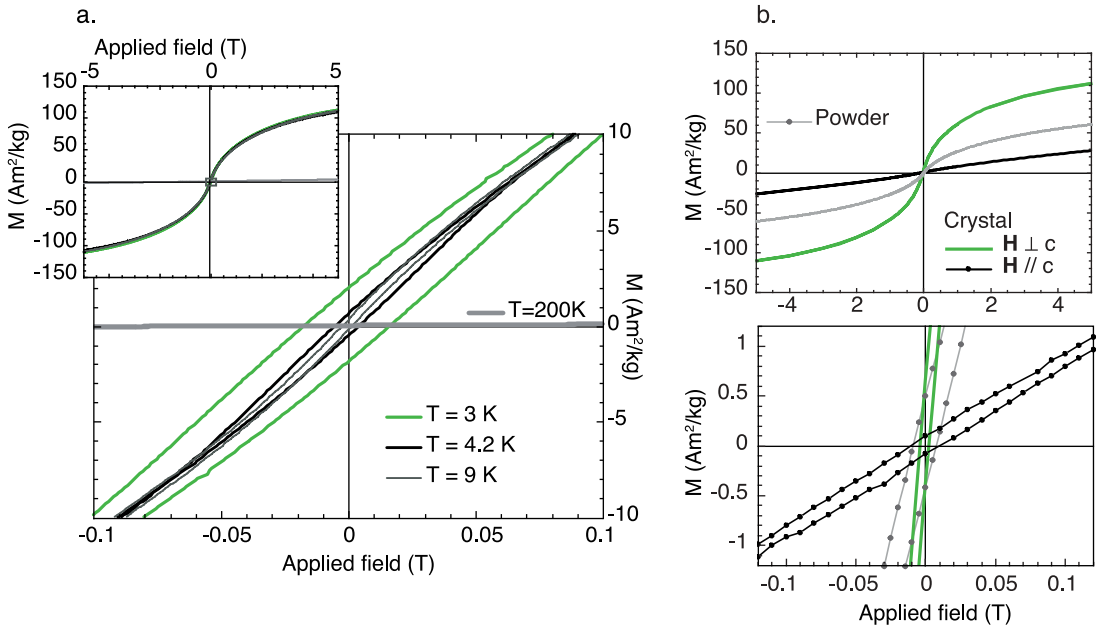

Figure 3. Hysteresis loops of (a) Salsigne crystal 2, with **H** perpendicular to the **c**-axis, at variable temperatures and of (b) Kisbanya powder and crystal 1, 2 orientations (T = 4.2 K).

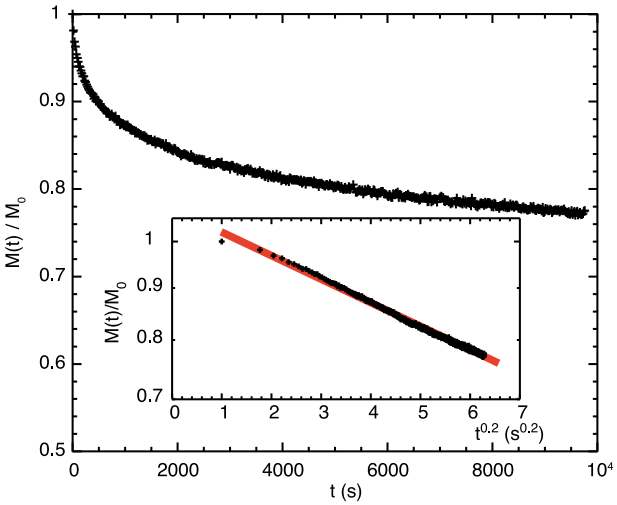

Figure 4. Thermoremanent magnetization of Kisbanya crystal 1 (**H** perpendicular to **c**, $T = 4$ K) acquired by cooling from RT to $T = 4$ K in a 0.5 mT applied field, measured after a waiting time of 1200 s (field on), and normalized to the initial remanence ($M_0 = 4.5 \times 10^{-3}$ Am^2/kg), versus t. Analogous although much noisier results were obtained with **H** applied along **c**. Inset shows logarithm of $M(t)/M_0$ plotted versus $t^{0.2}$, showing the stretched exponential nature of the curve: $M(t)/M_0 \propto \exp[-\text{const}*t^{0.2}]$ (fit: thick curve). The fitted exponent is in good agreement with values obtained in spin glasses [*Binder and Young*, 1986].

field is applied parallel to the **c**-axis, and 90% in the perpendicular case (Figure 3a). As a result of the strong magnetic anisotropy, the hysteresis loops obtained for the two orientations are markedly different, the curve obtained on a powder lying in-between (Figure 3b). In a powder sample from Przibram mine, measurements at 4.2 K along two perpendicular directions yielded differences of about 4% in M(5 T), and identical normalized loops, suggesting minor orientation effects. Results from high field measurements of terrestrial cronstedtite are reported in Table 3. Remanence in cronstedtite is unstable, and the slow decay of the thermoremanent magnetization with time (Figure 4) does not follow the exponential law predicted by Néel for the blocking of non-interacting single domain particles [*Néel*, 1949]. Instead, the relaxation can be fit to a stretched exponential (Figure 4). Such a behavior is frequently observed in spin glasses [*Fiorani*, 1992]. Relaxation processes are also demonstrated by the irreversibility of dc χ variations with T (Figure 2c). The splitting between ZFC and FC curves occurs just below the temperature of the maximum of ZFC, and the FC curve of single crystals has a plateau shape upon cooling. An increase of the applied magnetic field results in lowering the splitting temperature. These features are typical of glassy magnetic materials [*Mydosh*, 1993] and differ from the behavior of superparamagnets [*Bedanta and Kleemann*, 2009]. At high temperatures (150–300 K), once a temperature independent term χ_0 is substracted from the raw data, $1/(\chi - \chi_0)$ data fit to a straight line and follow a Curie-Weiss dependence (equation (1)). The temperature independent term is mostly due to core, sample holder and SQUID magnetometer background contributions. *Coey et al.* [1989] reported a significant electrical conductivity in cronstedtite. Thus, a paramagnetic Pauli susceptibility term due to delocalized electrons (see *Ashcroft and Mermin* [1976] for more details) might also contribute to χ_0. The effective moment μ_{eff} of powders, calculated using a fit to equations (1) and (2), is slightly lower than the spin-only ionic value $g.\{x.5/2.(5/2 + 1) + (1 - x).4/2.(4/2 + 1)\}^{1/2} \approx 5.4\ \mu_B$, with $g \approx 2$, the Lande factor and x, the proportion of ferric iron deduced from EMPA ($\mu_{eff} = 4.4$, 4.5 and 3.9 μ_B for Kisbanya, Salsigne and Przibram powders, respectively). We find, therefore, no evidence for macrospins, which would be observed in an assembly of ferromagnetic *s.l.* or antiferromagnetic nanoparticles, whether they interact, or not (see the review of *Bedanta and Kleemann* [2009]). The Curie-Weiss temperature is always lesser than 7 K and positive, suggesting weak and predominantly ferromagnetic interactions.

[16] The frequency dependence of ac susceptibility is illustrated in Figure 5a for Salsigne crystal 2. The position of the peak temperature varies with the frequency, and the imaginary part of the ac susceptibility completely vanishes above the maximum. Figure 5b illustrates, as does Figure 2c, the extreme sensitivity of the system to even small applied fields, which is a feature of spin glasses [e.g., *Mattsson et al.*, 1995]. Looking at the variations of the ac peak position among samples,

Figure 5. ac magnetic susceptibility measurements of crystals, **H** perpendicular to **c**. (a and b) (top) In phase and (bottom) out of phase components of χ_{ac} as a function of temperature, for different frequencies (Figure 5a, Salsigne crystal 2) and for different applied dc fields (Figure 5b, Salsigne crystal 1, 30 Hz frequency of the ac field). The inset in Figure 5a shows the fit of the ln(ω) versus the inverse of χ' peak temperature data to an Arrhenius law: despite the goodness of the fit, it yields an unphysical value of $\tau_0 = 10^{-43}$ s. (c) Comparison of the variations of ac susceptibility versus temperature for the 5 crystals studied. Note that the data were obtained using a 10 Hz frequency for all crystals but Salsigne, crystal 1 (30 Hz).

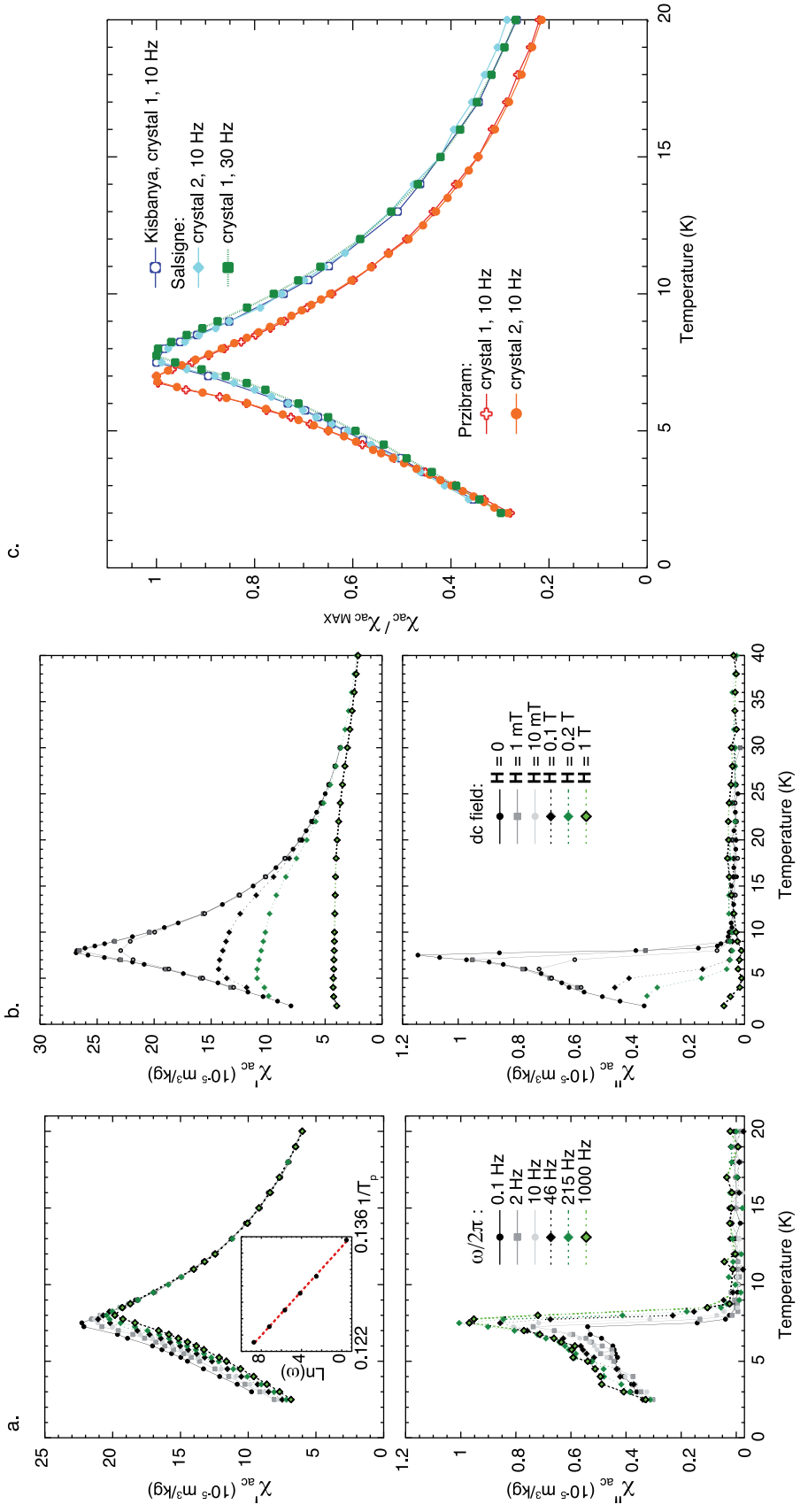
a.
b.
c.
χ'ac (10-5 m3/kg)
χ''ac (10-5 m3/kg)
Ln(ω)
0.122
0.136 1/Tp
ω/2π :
0.1 Hz
2 Hz
10 Hz
46 Hz
215 Hz
1000 Hz
dc field:
H = 0
H = 1 mT
H = 10 mT
H = 0.1 T
H = 0.2 T
H = 1 T
Temperature (K)
χac / χac MAX
Kisbanya, crystal 1, 10 Hz
Salsigne:
crystal 2, 10 Hz
crystal 1, 30 Hz
Przibram:
crystal 1, 10 Hz
crystal 2, 10 Hz

Figure 5

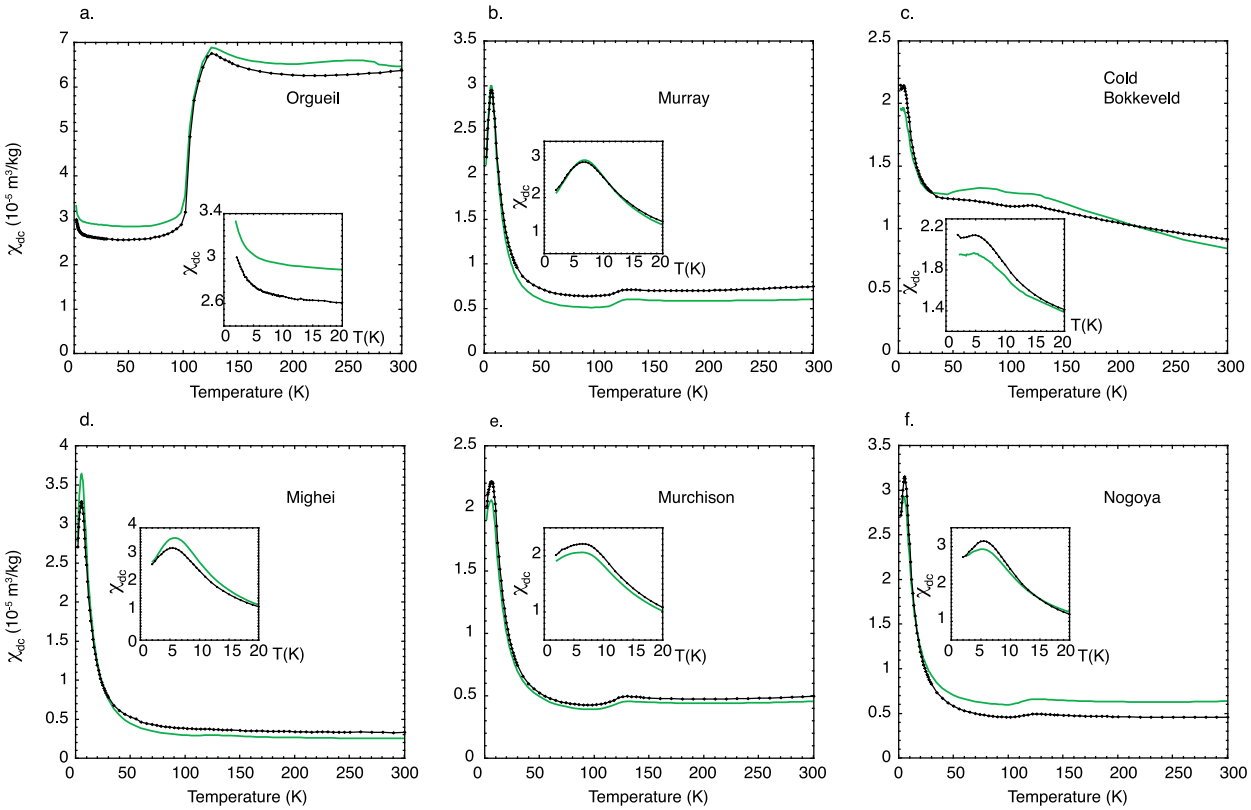

Figure 6. Evolution of the dc magnetic susceptibility (ZFC, 10 mT dc field) with temperature for the (a) Orgueil, (b) Murray, (c) Cold Bokkeveld, (d) Mighei, (e) Murchison, and (f) Nogoya chondrites. Results for two fragments are shown for each meteorite. Insets show zooms at low temperature.

which is better defined than the dc peak position, variations are minor when considering two crystals from the same mine, but significant among powders and crystals of the same mine, the former tending to have higher peak temperature values, by a maximum of ≈0.8 K (Table 3). Also, whereas the peak temperatures are nearly identical for Salsigne and Kisbanya samples, lower peak temperature values were obtained for samples from the Przibram mine (Table 3 and Figure 5c). These results suggest the interplay of grain size and crystal-chemistry on the position of the susceptibility peak.

4.2. Magnetic Properties of Chondrites

4.2.1. Orgueil, a CI Chondrite

[17] The magnetic properties of CM2 chondrites are best understood by comparison with the properties of Orgueil, a CI chondrite (Figure 6a). The Verwey transition of magnetite is well expressed in the dc susceptibility curves, although the corresponding temperature T_v is lower than 120 K, as previously noticed [*Thorpe et al.*, 2002]. This result confirms the predominance of magnetite in the room temperature (RT) magnetic signal of Orgueil [*Rochette et al.*, 2008]. Below 10 K, the susceptibility increases as the temperature decreases down to 2 K, suggesting the predominance of a paramagnetic component at low temperature, likely due to phases containing magnetically diluted Fe, or Ni. The signature of Fe-rich serpentines is not identified, suggesting that if any, they do not predominate the phyllosilicate assemblage. This is in agreement with mineralogical studies of Orgueil, suggesting the predominance of Fe-bearing Mg-serpentine and especially, Fe-bearing saponite-serpentine phases [*Tomeoka and Buseck*, 1988; *Bland et al.*, 2004].

4.2.2. Murray, a CM2 Chondrite

[18] In contrast to Orgueil, the dc susceptibility of the Murray chondrite (Figure 6b) presents a peak at ≈7 K, which can be attributed to Fe-rich phyllosilicates, mostly serpentines (see Introduction). The Verwey transition of stoichiometric magnetite, at T ≈ 120 K, is visible in Murray, but the corresponding

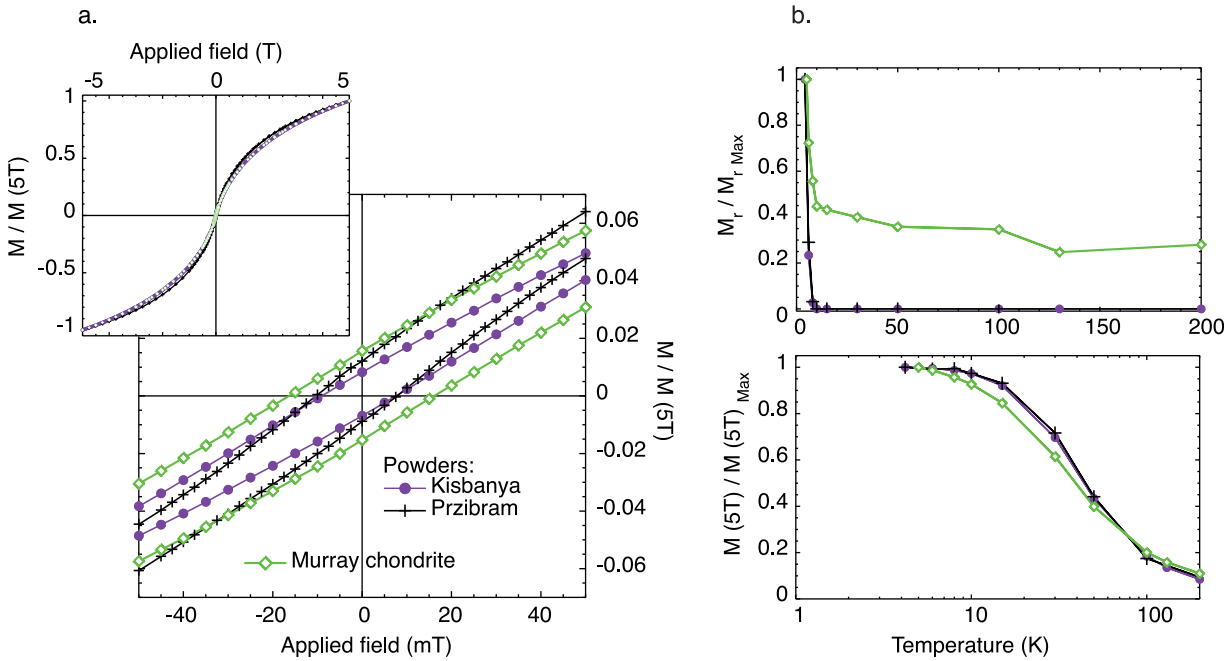

Figure 7. (a) Normalized hysteresis loop of the Murray chondrite measured at $T = 4.2$ K, compared with cronstedtite powders: (top) entire loops and (bottom) zoom. (b) Evolution of (top) M(5 T) (normalized to the maximum) and of (bottom) M_r (normalized to the maximum) with T in Murray, compared with results from powder cronstedtite.

susceptibility jump is fairly small in comparison with Orgueil, due to the much lower content of magnetite [*Hyman and Rowe*, 1986]. We observe differences between the 2 fragments (Figure 6b), reflecting mineralogical differences and/or sample heterogeneities. However, the average RT susceptibility values we find here for Orgueil and Murray (average of the 2 fragments) are only 0.6% and 1.4% different, respectively, from the values obtained by *Rochette et al.* [2008] on large fragments ($m > 100$ g). The positions of the low-T peaks (within a ± 0.5 K interval for the 2 fragments) are within the range of observations for cronstedtite in the same experimental conditions.

[19] The global shape of the normalized hysteresis loop obtained on the Murray chondrite at 4.2 K is comparable to that of powder cronstedtite samples (Figure 7a). The value of M(5 T) for Murray is lower than that of cronstedtite, which can be explained at first order by the dilution of Fe-rich serpentines by other, non-magnetic phases in Murray. Decreasing the temperature from 100 K to 5 K results in a progressive opening of the hysteresis cycle, with increasing M_r (Figure 7b), consistent with cronstedtite's behavior. The Verwey transition is expressed by a slight decrease of M_r with T, whereas is it not visible in the M(5 T) variations, as observed in magnetite [*Özdemir and Dunlop*, 1999]. Therefore, the low-T magnetic signature of Murray chondrite reflects that of magnetite, which predominates above 120 K, and Fe-serpentine close the Fe end-member cronstedtite, which predominates at lower temperatures.

4.2.3. Other CM2 Chondrites

[20] The comparison of the dc susceptibility curves of a series of five CM2 chondrites is shown in Figure 6. The Verwey transition of magnetite is always observed but it occurs at variable temperatures (Table 4). Changes in susceptibility across the transition are always moderate. An additional, broad feature is also observed in one of the Cold Bokkeveld fragments, peaking around 75 K. Molecular oxygen exhibits a series of phase and magnetic transitions between 70 K and 30 K, which might be a concern, especially when measuring low magnetic moments (moments of the order of 10^{-7} Am^2 at 70 K in this case). We checked, however, by repeated measurements of this sample and a paramagnetic reference, that it was not a measurement artifact. All curves show evidence for low-T susceptibility peaks attributed to Fe-serpentines, which are abundant in all of them (e.g., *Browning et al.* [1996]) with, however, markedly different features and positions (Figures 6b–6f and Table 4), best seen on the ac susceptibility curves (Figure 8). Murchison presents a broad feature that appears to

Table 4. Magnetic Properties of CM2 Chondrites

		Susceptibility Measurements[a]						Hysteresis Measurements[e] (T = 4.2 K)		
	m (mg)	T_p dc[b] (K)	T_v dc (K)	χpeak[b]	χ(2 K)[b]	χ(RT)[b]	T_p ac, K	M(5 T)	M_r	H_c
Cold Bokkeveld										
1	7.49	4.75 (±0.25)	≈114 K	2.1	2.2	0.9	6.5 (±0.25)	24.41	0.69	34.9
2	0.63	4.75 (±0.5)	n.o.	2.0	2.0	0.8	n.d.	23.18	0.77	43.2
Mighei										
1	5.41	5.75 (±0.25)	≈118 K	3.6	2.8	0.3	6.7 (±0.2)	30.22	0.24	7.3
2	1.53	5.5 (±0.25)	n.o.	3.3	2.7	0.3	n.d.	29.12	0.20	7.0
Murchison[c]										
1	6.12	<6/6.5 (±0.5)	≈118 K	2.1	1.9	0.5	≈4.5/7.5 (±0.25)	23.92	0.38	20.6
2	5.85	<6/6.5 (±0.5)	≈118 K	2.2	2.0	0.50	≈4.5/7.4 (±0.2)	24.95	0.41	20.4
Murray										
1	5.36	6.75 (±0.25)	≈120 K	3.0	2.1	0.6	7.5 (±0.25)	27.06	0.42	16.3
2	1.35	6.75 (±0.25)	≈120 K	3.0	2.2	0.7	7.4 (±0.2)	26.88	0.45	17.7
Nogoya										
1	6.09	5.2 (±0.2)	≈113 K	2.9	2.7[d]	0.6	6.5 (±0.25)	25.40	0.24	8.8
2	3.55	5.5 (±0.25)	≈114 K	3.2	2.7	0.5	6.4 (±0.2)	26.94	0.27	9.0

[a]Susceptibility: χ: in 10^{-5} m^3/kg; peak: at T_p: peak temperature. ac measurements: frequency: 10 Hz; n.d.: signal too weak to be measured.
[b]dc measurements obtained using an induction of 10 mT. T_v: Verwey temperature, at which the derivative of the sample's moment with respect to T is at a maximum. (n.o.: not observed, signal noisy).
[c]Murchison's T_p values: the first figure stands for the secondary peak.
[d]T = 2.5 K.
[e]Hysteresis: M: magnetization at 5 T, Am^2/kg; M_r: remanence, same unit; H_c: coercive force, mT.

be due to a secondary lower temperature (≈5 K) peak visible on ac curves. The hysteresis loops of the series of CM2 studied (the 2 fragments of a meteorite yield nearly identical results) at 4.2 K, normalized to M(5 T) show very similar features (Figure 9). Cold Bokkeveld has a maximum opening, likely related to the supplementary phase identified. In addition, although the variation of M (5 T) with temperature is comparable to that of Murray, the decrease of M_r with temperature is smoother (Figure 9b).

5. Discussion

5.1. Spin-Glass Like Behavior in Cronstedtite

[21] A susceptibility peak is observed in cronstedtite single crystals near 7 K, which sharpens for ac susceptibility, and a split between zero field cooling and field cooling is seen below the maximum (Figures 2 and 5), suggesting a magnetic freezing [*Mydosh*, 1993]. In addition, the peak height of ac susceptibility increases and shifts to lower temperatures with decreasing frequency (Figure 5a). The frequency shift p per decade ω, the angular frequency, defined as $p = \Delta T_p/[T_p \Delta \log(\omega)]$ [after *Mydosh*, 1993] takes values between 0.02 and 0.03 for cronstedtite crystals and powders, similarly to many spin-glasses. This shows a dependence consistent with cooperative freezing rather than blocking of superparamagnetic particles (≈0.3) or a long-range order transition [*Mydosh*, 1993]. This is consistent with neutron diffraction data showing the lack of long-range ordering [*Elmaleh et al.*,

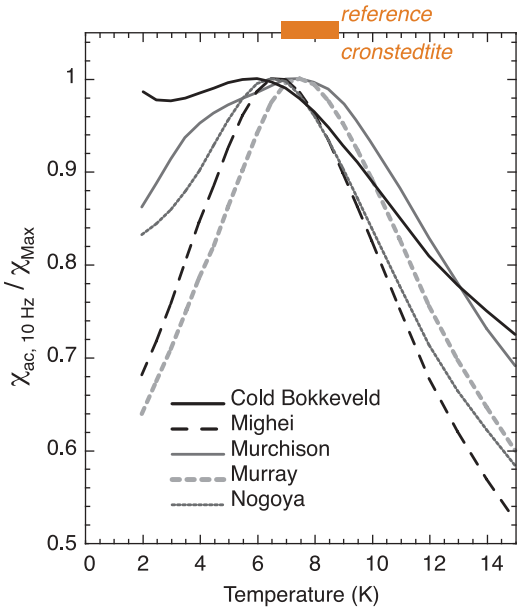

Figure 8. Low temperature ac susceptibility of the 5 CM2 chondrites. The rectangle corresponds to the range of variation of the peak temperature measured in the same conditions in the reference cronstedtite samples.

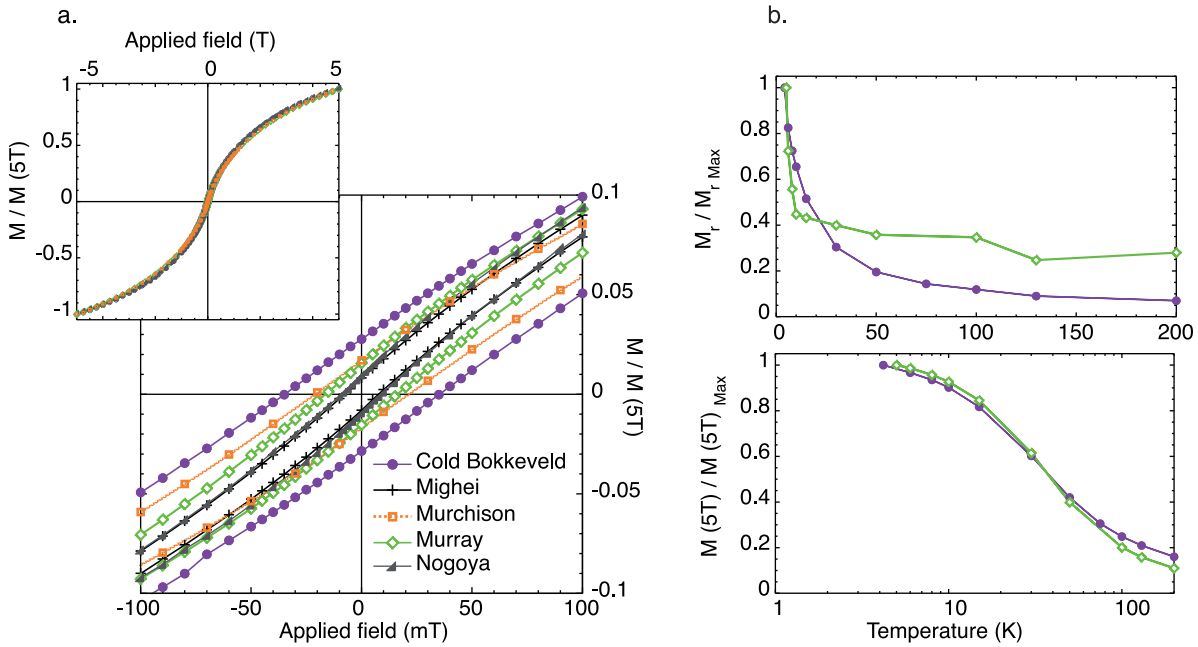

Figure 9. (a) Normalized hysteresis loops of the 5 CM2 chondrites measured at T = 4.2 K: (top) entire loops and (bottom) zoom. (b) Evolution of (top) M(5 T) (normalized to the maximum) and of (bottom) M_r (normalized to the maximum) with T in the Cold Bokkeveld chondrite, compared with results from the Murray chondrite.

2010; A. Elmaleh et al., manuscript in preparation, 2012]. The magnetic behavior at $T \gg T_p$ yields no evidence for a giant effective moment. This further suggests that T_p does not correspond to the blocking temperature of non-interacting fine particles. This is confirmed by the variation of the peak temperature of ac susceptibility with the frequency. Indeed, the fit of these data to an Arrhenius law of the form: $\tau/\tau_0 = \exp(Ea/k_B{*}T)$ ($\tau = 1/\omega$, Ea: activation energy) yields unphysical values of the relaxation time τ_0 (from 10^{-20} s down to 10^{-43} s). Thus the magnetic behavior cannot be attributed to nano-oxides formed by weathering or present as inclusions, as observed in some natural silicates [*Belley et al.*, 2009]. In addition, SCXRD shows that all the analyzed crystals are monophasic. No spurious diffraction spots or rings giving evidence of the presence of other mono- or poly crystalline materials are observed. Backscattered electrons images (EMP) also showed homogeneous samples. The properties measured would rather suggest a spin-glass behavior in cronstedtite. Such a behavior may occur in concentrated assemblies of individually responding magnetic nanoparticles, yielding a transition from a superparamagnetic state to a disordered collective state (superspin-glass state), as observed for instance in concentrated ferrofluids made of maghemite nanoparticles dispersed in water [*Parker et al.*, 2008]. The absence of a giant effective moment in this magnetically concentrated system rather suggests that the observed behavior is the result of the frustration of magnetic interactions in the bulk material.

[22] At 4.2 K, in 5 T, the Brillouin functions (the expression is given by *Ashcroft and Mermin* [1976]) for S = 5/2 Fe^{3+} and S = 2 Fe^{2+} yield magnetizations of ≈257 and 200 Am^2/kg respectively. Magnetization of non-interacting assemblies containing between 38 and 43% of ferric iron would lead to magnetizations of ≈220 Am^2/kg. The high field part of all magnetization curves falls well below Brillouin curves (Table 3). Thus, there must be strong antiferromagnetic interactions suppressing the magnetization at low temperature. Previous studies of phyllosilicates containing only ferrous or ferric iron suggest that octahedral Fe^{3+} ions are antiferromagnetically coupled and Fe^{2+} ions, ferromagnetically coupled, as reviewed by *Ballet et al.* [1985]. In cronstedtite's octahedral layer, 73 to 80% of the cations are ferrous ions, which ferromagnetic interactions would explain the slightly positive Curie-Weiss temperature measured in powders. The remaining ferric iron ions are distributed among the triangular array of cations. Frustration among spins is expected to arise from the competition between the ferromagnetic and antiferromagnetic bonds within each octahedral layer, as suggested for 2:1:1 Fe-phyllosilicates by *Ballet et al.* [1985]. Tetrahedral ferric iron might

further disrupt long-range magnetic ordering, since there is no evidence for Si-Fe ordering in tetrahedral layers [*Hybler et al.*, 2000]. It is not easy to evaluate separately the impact of octahedral and tetrahedral Fe^{3+} on the magnetic properties of cronstedtite, as charge balance imposes that they are present in equal amounts. Further studies of synthetic crystals with various sites occupancies by Fe^{3+} would bring further insight into the mechanisms inducing the glassy behavior of cronstedtite.

5.2. Influence of Grain Size and Composition on the Magnetic Signature of Cronstedtite

[23] The position of T_p, taking all samples and measurement positions, and for a given procedure, encompasses a maximum range of the order of 1.5 K (≈21% variation of T_p) (Table 3). Powders gave systematic differences (higher T_p) when compared to their crystal counterparts. Samples from Kisbanya and Salsigne have higher peak temperatures than crystals from Przibram (Table 3), as clear from the more precise ac data (Figure 5c). Several parameters, often depending on one another, might be involved here. The predominant polytype can apparently be ruled out, because the crystals studied were refined in the *P*31*m* space group (1*T* polytype, Table 2). No independent estimate of the redox state of iron is available. The impact of this parameter cannot therefore be properly addressed. However, considering the estimates made from EMPA on the assumption of the lack of vacancies in the structure (Table 1), which has been suggested by previous crystallographic studies of 1*T*-cronstedtite [*Hybler et al.*, 2000], no systematic variation of T_p is observed with that parameter. The most obvious difference between Salsigne and Kisbanya samples on the one hand, Przibram samples on the other hand, is the chemical composition. The former have almost no impurity (Table 1) whereas the latter have significant amount of substitution of Fe by Mg mostly, with only minor amounts of Mn. This suggests a possible effect of diamagnetic substitution of Fe on the magnetic properties. In concentrated systems, diamagnetic impurities can degenerate spin configurations and increase frustration [*Binder and Young*, 1986]. At the same time, although relatively small, there are variations of the degree of disorder of the crystals. Both BASF values (Table 2) and the diffuse streaks along the non-family reflections rows (Figure 1) suggest that Przibram crystals are slightly more disordered than Salsigne and especially Kisbanya crystals. Przibram crystal 2 is fractured and therefore more disordered than crystal 1, as visible from Figure 1, so that it is not straightforward to draw conclusions on the effect of disorder. More work is needed to ascertain the evolution of the peak position with grain size, interactions, disorder and crystal-chemistry, but the present results give a first estimate of the range of variations of T_p, which lower bound is well defined, and suggest possible causes for its evolution.

[24] A prominent feature of the oriented crystals studied is the strong magnetic anisotropy, with a hard **c**-axis. High field measurements made on Salsigne crystal 2 at different positions with the magnetic field applied in the (001) plane yield negligible differences in the magnetization values (<5%). The strong magnetic anisotropy of cronstedtite has two consequences. First, since it is highly enhanced at low temperature, it gives the possibility to better evaluate the orientation of Fe-rich serpentines in CM2 chondrites than at RT. Second, the use of magnetization values for identification and quantification purposes would require that this effect is properly taken into account. Powders can help to solve this problem. However, grain size and magnetostatic interactions between the grains can modify magnetization values, especially hysteresis parameters, while low-field susceptibility is less affected [*Carter-Stiglitz et al.*, 2001]. Here we observe a systematic increase in the opening of the hysteresis cycles in concentrated powders. The whole data set suggests that, however, only a small opening of the hysteresis cycle is observed ($Hc < 13$ mT and $M_r < 1$ Am^2/kg) and that the remanent magnetization almost entirely collapses when the temperature is raised just above T_p to ≈10 K, which is typical of a spin-glass. These characteristics can be considered as index features of the mineral.

5.3. Low-Temperature Magnetic Mineralogy of CM2 Chondrites

[25] In the 5 meteorites studied, the Verwey transition of magnetite and a low temperature susceptibility peak, which is not seen in the Orgueil CI chondrite signal, have been identified (Figures 6 and 8). An additional broad feature centered around 75 K was observed in Cold Bokkeveld, which attribution is not straightforward. To our knowledge, among the major Fe and Ni bearing of CM2 chondrites, some have not been characterized magnetically at low-*T* (tochilinite), many others exhibit low-*T* χ variations that would be not compatible with any of the features observed here (pentlandite [*Knop et al.*, 1976];

pyrrhotite [*Rochette et al.*, 1990]; Fe-rich pyroxene [*Eeckhout et al.*, 2001]; Fe-rich olivine [*Belley et al.*, 2009]; Fe, Ni-alloys [*Kohout et al.*, 2007]). *Kohout et al.* [2007] observed a low-field susceptibility peak at ≈70 K in ordinary chondrites, which they attributed to a transition of troïlite (FeS) toward a weak antiferromagnetic state at low temperatures. *Gattacceca et al.* [2011] suggested that it was rather the signature of chromite, which is also encountered as an accessory phase in CM chondrites [*Johnson and Prinz*, 1991; *Lauretta et al.*, 2000]. The variation of M_r with T for chromite [*Gattacceca et al.*, 2011, Figure 2] would provide an explanation for the smooth decrease observed here (Figure 9b). Whatever the nature of this phase, it is likely to contribute to the susceptibility decrease observed in Cold Bokkeveld fragments at $T > Tv$. As a consequence, estimates of the amount of magnetite in this meteorite using its RT susceptibility can be questioned. On the contrary, the signature of magnetite would predominate the RT signal of the other CM2 and CI studied, as previously suggested [*Hyman and Rowe*, 1986; *Thorpe et al.*, 2002; *Rochette et al.*, 2008]. The width of the anomaly associated with the Verwey transition is larger than 15 K. Variations in stress affect the temperature of the Verwey transition, and stress fields around dislocations may result in large transition widths [*Muxworthy and McClelland*, 2000]. The large transition width may also indicate variations in composition. The position of the transition varies from ≈120 K to 113–114 K among the CM2 chondrites (Table 4). T_v can be lowered either by reducing the particle size [*Prozorov et al.*, 2007], by substitution of Fe by a diamagnetic or an alternative paramagnetic ion, or by oxidation. A 5–10 K drop in T_v would correspond to the oxidation of about 2–4 ‰ Fe [*Kąkol and Honig*, 1989] or to the substitution of 0.4–0.8% Fe by Ni [*Brabers et al.*, 1998]. *Palmer and Lauretta* [2011] observed magnetite grains with less than 1.5% substitution of Fe by Ni, compatible with T_v, as well as Ni richer iron oxides with a lower Fe^{3+} content in Murchison, Murray and Cold Bokkeveld. In their study, no iron oxides were observed in Nogoya. The present results suggest that in average, the signature of nearly stoichiometric magnetite predominates the signal of Mighei, Murchison, Murray and Nogoya at RT, and illustrates the complementarity between the magnetic approach and discrete analyses. Using the expression of *Rochette et al.* [2008] linking χ at RT to the mass magnetite content we find 0.57% ± 0.23, 0.93% ± 0.12, 1.32% ± 0.41 and 1.07% ± 0.48 magnetite, respectively (average, 2σ) in good agreement with previous estimates from magnetic measurements [*Hyman and Rowe*, 1986] and by XRD of Murchison [*Bland et al.*, 2004]. The values obtained by *Howard et al.* [2009] (XRD) are systematically higher, but the two sets of data are compatible within error. Our estimates are made on small fragments of heterogeneous brecciated chondrites [*Rubin et al.*, 2007]. Thus, larger fragments would be more representative of the whole meteorite [*Rochette et al.*, 2008].

[26] At $T < T_v$ the magnetic susceptibility of Mighei, Murchison, Murray and Nogoya appears to be mostly composed of that of Fe-rich serpentines and magnetite, which can be considered as nearly steady below about 100 K to a first approximation [*Muxworthy*, 1999; *Prozorov et al.*, 2007]. In the Murray chondrite, the position of the low-T peak is close to that of cronstedtite. If we consider that the contribution of magnetite at 2 K is equal to the magnetic susceptibility at 100 K, the contribution of Fe-serpentines would be about 1.7×10^{-5} m^3/kg by difference, using the fact that low-field susceptibilities of phases in a mixture are, to first order, additives [e.g., *Carter-Stiglitz et al.*, 2001]. Taking ≈50 wt% Fe-rich serpentines in Murray [*Howard et al.*, 2009] yields an intrinsic susceptibility $\chi \approx 3.2 \times 10^{-5}$ m^3/kg at 2 K. This value is within the interval measured in cronstedtite, in particular in powders ($\chi \approx 2.6$ to 5.1×10^{-5} m^3/kg). The contribution of paramagnetic phases or the possible contribution of tochilinite are difficult to evaluate, but at present, it seems reasonable to assume that Fe-rich serpentines close to cronstedtite are the main minerals contributing to the magnetic susceptibility peak(s) observed in Murray below 7 K. The frequency-sensitivity parameter p of ac data is equal to ≈0.03, as in cronstedtite powders, which supports this hypothesis. At RT, $\chi_{cronstedtite} \approx 0.2 \times 10^{-5}$ m^3/kg, inducing an error of ≈15% on the estimate of the magnetite content from RT χ measurements. In Mighei, Nogoya and Cold Bokkeveld, T_p is out of the range of reference cronstedtite. Also, low p values are found for these meteorites, but whereas it is ≈0.03 in Mighei, it has higher values in Nogoya (≈0.05) and Cold Bokkeveld (≈0.07). It suggests that this peak is due to Fe-rich phyllosilicates, most likely serpentines, with composition and possibly structures that differ from that of the reference cronstedtite studied. Murchison is characterized by a peak, which position is close to that of Murray and with a p value ≈0.03, as well as by a secondary one at lower temperature. A fuller understanding of the role of crystallinity and grain size would be important here, to separate these effects from compositional effects. At present, our

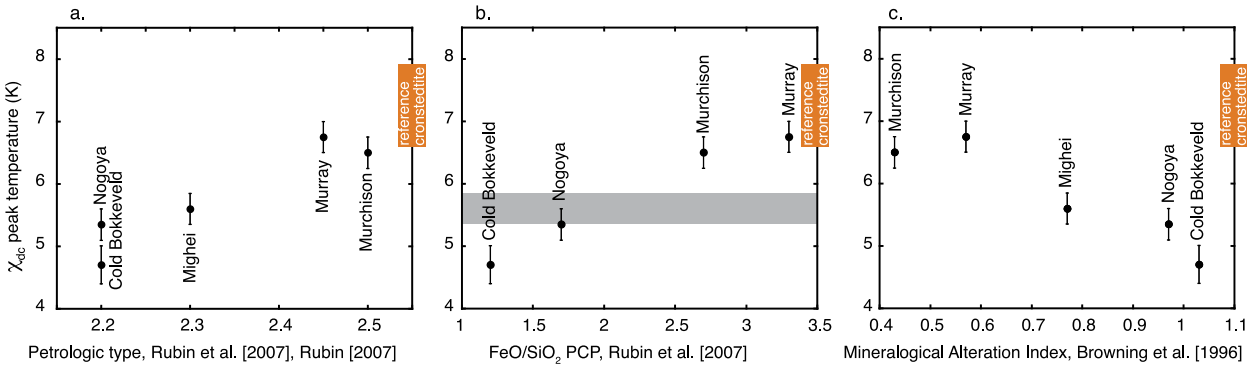

Figure 10. Evolution of the temperature of the dc peak susceptibility temperature of CM2 chondrites with (a) the petrologic type, related to the degree of alteration [*Rubin*, 2007; *Rubin et al.*, 2007]; (b) the relative content of iron and silicon, in oxide wt%, in PCP [*Rubin et al.*, 2007] (no data are available for the Mighei chondrite, for which peak temperature within error is indicated by a gray band); and (c) the degree of alteration according to the Mineralogical Alteration Index (MAI) [*Browning et al.*, 1996]. The interval representing data from reference samples of cronstedtite is indicated by a rectangle.

results on reference cronstedtite suggest that T_p increases as the grain size is reduced. Therefore, even though grain size might play a role in the evolution of T_p among chondrites, the fact that we observe lower peak temperatures for most CM2 chondrites with respect to reference cronstedtite suggests a compositonal effect rather than a grain size effect.

5.4. Evolution of the Low-*T* Magnetic Signature of CM2 Chondrites With Their Degree of Alteration

[27] Several alteration scales have been proposed for CM2 chondrites [*Browning et al.*, 1996; *McSween*, 1979; *Rubin et al.*, 2007]. They take into account the amount of Fe in serpentines. The alteration scale of *Rubin et al.* [2007] is based on several other parameters including the Mg content of Ca-carbonates. Thus, it is interesting to start by comparing our results to that composite alteration scale (Figure 10a). Despite some discrepancies, an overall correlation is observed: T_p increases with the petrologic type, which is inversely correlated to the degree of alteration. In *Rubin et al.* [2007] as well as in most other alteration studies, Murray and Cold Bokkeveld, which have the most contrasted T_p values, are considered to have recorded two extreme degrees of alteration. An important consequence is that measuring the low-*T* magnetic properties of CM2 chondrites appears as a method to evaluate their degree of alteration. Since it is possible to measure mm size fragments, the heterogeneity of a meteorite can be evaluated at the mm scale. This has proven useful in the case of the Paris chondrite, a newly discovered CM chondrite [*Zanda et al.*, 2010], showing differences in the low-*T* magnetic properties of clasts with different degrees of alteration [*Elmaleh et al.*, 2011]. The double low-*T* peak in the Murchison chondrite suggests a lower-scale heterogeneity and the coexistence of two populations of Fe-serpentines. It might correspond to populations of serpentines having different sizes and morphologies, as observed by TEM in CM2 chondrites [*Lauretta et al.*, 2000] and/or to a fine scale chemical heterogeneity.

[28] Two major difficulties reside in the comparison between the magnetic signature of Fe-rich serpentines and mineralogical data: the dispersion of the compositions measured [*Zolensky et al.*, 1993] and the scarcity of high resolution data (TEM-EDS). The resolution of TEM analyses is, however, required in order to determine the serpentines' mineralogy rather than averages over an unknown number of given compositions. Most studies are based on EMPA. They generally agree on the fact that the phyllosilicates or the phyllosilicate-rich assemblages are decreasingly Fe-rich and conversely, Mg-richer, with the degree of alteration [*McSween*, 1979; *Tomeoka and Buseck*, 1985; *Browning et al.*, 1996; *Palmer and Lauretta*, 2011]. Figures 10b and 10c show the comparison between the evolution of T_p among CM2 chondrites, the FeO/SiO_2 ratio of PCP [*Rubin et al.*, 2007] (no data are given on Mighei), and the Mineralogical Alteration Index [*Browning et al.*, 1996]. The latter measures the Fe^{3+} content of serpentines in the fine-grained matrix and, therefore, evaluates the proximity to the Fe end-member cronstedtite, where Fe^{3+} substitutes Si. In both cases, the good agreement suggests a link between Fe incorporation in Fe-

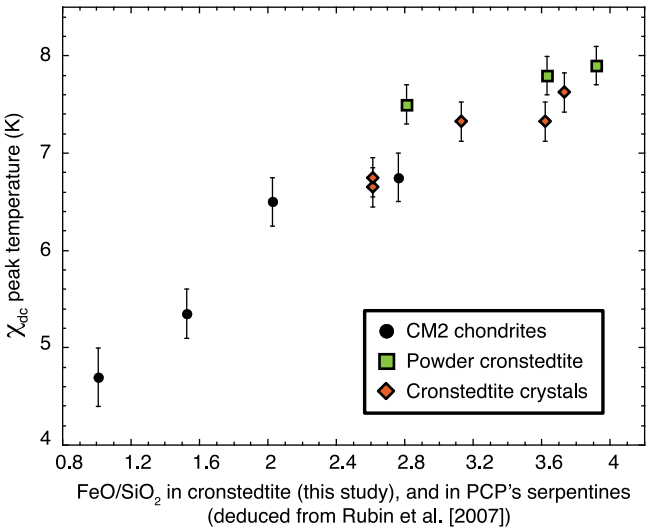

Figure 11. Evolution of T_p measured for the 5 CM2 chondrites and for reference cronstedtite samples, with the FeO/SiO_2 wt% measured (EMPA, this study) or the FeO/SiO_2 ratio of PCP determined by *Rubin et al.* [2007] corrected for mono-sulfides using the corresponding S wt% analyses [*Rubin et al.*, 2007].

serpentines and the position of the susceptibility peak. Based on TEM-EDS data from Cold Bokkeveld chondrite and previous unpublished data, *Zega and Buseck* [2003] concluded that the Mg content of Fe-rich serpentines in this meteorite is higher than in Murchison chondrite. Variations of T_p might therefore reflect the Fe/(Fe + Mg) content of the predominant Fe-rich serpentines, and not only the mixing of Fe-rich and Mg-rich serpentines in various proportions. We observed a high anti-correlation between the PCP MgO wt% from *Rubin et al.* [2007] and T_p (R^2 = 0.99, not shown here) whereas Al_2O_3 wt% and T_p are not so strongly anti-correlated (R^2 = 0.57). *Rubin et al.* [2007] outlined the influence of sulfide phases, most likely tochilinite, in the value of the FeO/SiO_2 ratio. A simplistic correction was applied by subtracting the contribution of a mono-sulfide phase. The correlation between the corrected data and T_p is shown on Figure 11. Data from cronstedtite crystals (compositional data are from EMPA on each crystal) and powders (mine means) are also shown. The correlation observed (R^2 = 0.90) strongly supports the influence of chemistry on T_p values. In the Cold Bokkeveld chondrite, the magnetic susceptibility increases at $T < T_p$ (Figure 6), suggesting the predominance of a paramagnetic phase at 2 K. This observation is in good agreement with *Howard et al.* [2009] who showed that Mg-rich serpentines (which always contain magnetically diluted Fe impurities) predominate over Fe-rich serpentines in this meteorite, in contrast with the other four. The influence of the substitution of Si or Fe by Al, observed in various CM2 chondrites [*Zolensky et al.*, 1993], the role of crystallinity and grain size (evaluated using well-sorted cronstedtite powders), and of the presence of tochilinite on the low-T magnetic signature of chondrites now need to be fully addressed, in order to better understand the parameters influencing its evolution with the degree of alteration.

6. Conclusions

[29] Two major conclusions can be drawn from this study of the magnetic properties of the Fe-rich serpentine cronstedtite and of CM2 chondrites. First, the relaxation behavior of pure or Mg-substituted cronstedtite, characterized by SCXRD and EMPA, suggests that the mineral is characterized by a random-type short range magnetic order at low-T giving rise to magnetic hysteresis below ≈10 K, a sharp susceptibility peak at ≈7 K as well as fast and slow relaxation processes below the peak temperature. This glassy behavior is attributed to conflicting ferromagnetic and antiferromagnetic interactions within octahedral layers, with a possible role of the random distribution of ferric iron in tetrahedral layers. Even though further work is needed to fully understand the dynamic of this system and its evolution with substitutions, grain size and the interactions between the grains in a powder, the present study clarifies the nature of the magnetic order, and provides an attempt to identify the low-T signature of the mineral and its

variations, which can be used as a reference for studying rock samples. Second, the usefulness of rock magnetic techniques to the investigation of Fe-rich serpentines mineralogy is illustrated by the results obtained on a series of CM2 chondrites. The signature of Fe-serpentines, as well as its evolution with the degree of alteration of the chondrites, are identified, with variations of ≈30% in the position of the magnetic susceptibility peak. Low-*T* rock magnetic techniques can, therefore, provide a quick method to sort the numerous meteorites falls, and finds. Bulk magnetic methods are clearly blind to any accessory Fe- or Ni- bearing phase, which highlights the need for direct methods for studying the whole Fe-rich alteration assemblage in meteorites. However, they bring a complementary insight by giving estimates of the bulk Fe-serpentines mineralogy. Studies of terrestrial serpentinization have shown that the incorporation of Fe in serpentines depended on the conditions of the reaction (temperature, water:rock ratio [*Klein et al.*, 2009]) and on their duration [*Marcaillou et al.*, 2011]. A good understanding of hydrothermal alteration processes on Earth and on asteroids relies, therefore, on a thorough characterization of the Fe-content of serpentines. Using EMPA and SCXRD of single crystals of cronstedtite, we suggest that the substitution of Fe by Mg in cronstedtite modifies the magnetic signature. Increased substitution of Fe by Mg in meteoritic cronstedtite with the degree of alteration might therefore explain the evolution of their low-*T* magnetic properties. Finally, the magnetic study of oriented cronstedtite crystals shows the strong anisotropy of the mineral at low-*T* due to Fe^{2+} single-ion anisotropy. The low-*T* magnetic fabric of Fe-serpentine bearing chondrites may, therefore, be a powerful tool for studying deformation events caused by impact or compaction. Indeed, a recent study [*Lindgren et al.*, 2011] has shown that CM2 chondrites may have encountered several episodes of deformation during and after aqueous alteration events.

Acknowledgments

[30] We are thankful to J.-C. Boulliard and B. Zanda for the curation of the samples (minerals and meterorites, respectively) and for fruitful discussions. V. Dupuis, R. Hewins, J.-L. Robert, P. Sainctavit and F. Gendron are also thanked for helpful discussions. We thank J. Brest for technical support, Y. Li, Y. Zheng and F. Lagroix (IPGP) for their help with the MPMS and Y. Dumont, with the PPMS (GEMAC). We thank the Editor, J. Tyburczy, the Associate Editor, as well as A. Muxworthy and an anonymous referee, for their comments that significantly improved an earlier version of this manuscript. This work was funded by the ANR project JC 0503 1 (2010).

References

Ashcroft, N. W., and N. D. Mermin (1976), *Solid State Physics*, Saunders Coll., Philadelphia, Pa.

Bailey, S. W. (1969), Polytypism of trioctahedral 1:1 layer silicates, *Clays Clay Miner.*, *17*, 355–371, doi:10.1346/CCMN.1969.0170605.

Ballet, O., J. M. D. Coey, and K. J. Burke (1985), Magnetic properties of sheet silicates 2:1:1 minerals, *Phys. Chem. Miner.*, *12*, 370–378, doi:10.1007/BF00654348.

Beck, P., et al. (2010), Hydrous mineralogy of CM and CI chondrites from infrared spectroscopy and their relationship with low albedo asteroids, *Geochim. Cosmochim. Acta*, *74*, 4881–4892, doi:10.1016/j.gca.2010.05.020.

Bedanta, S., and W. Kleemann (2009), Supermagnetism, *J. Phys. D Appl. Phys.*, *42*, 013001, doi:10.1088/0022-3727/42/1/013001.

Belley, F., E. C. Ferré, F. Martín-Hernández, M. J. Jackson, M. Darby Dyar, and E. J. Catlos (2009), The magnetic properties of natural and synthetic $(Fe_x, Mg_{1-x})_2SiO_4$ olivines, *Earth Planet. Sci. Lett.*, *284*, 516–526, doi:10.1016/j.epsl.2009.05.016.

Binder, K., and A. P. Young (1986), Spin glasses: Experimental facts, theoretical concepts and open questions, *Rev. Mod. Phys.*, *58*, 801–976, doi:10.1103/RevModPhys.58.801.

Bland, P. A., G. Cressey, and O. N. Menzies (2004), Modal mineralogy of carbonaceous chondrites by X-ray diffraction and Mössbauer spectroscopy, *Meteorit. Planet. Sci.*, *39*, 3–16, doi:10.1111/j.1945-5100.2004.tb00046.x.

Blessing, R. H. (1995), On the differences between X-ray and neutron thermal vibration parameters, *Acta Crystallogr., Sect. B Struct. Sci.*, *51*, 816–823, doi:10.1107/S0108768194012474.

Brabers, V. A. M., F. Walz, and H. Kronmüller (1998), Impurity effects upon the Verwey transition in magnetite, *Phys. Rev. B*, *58*, 14,163–14,166, doi:10.1103/PhysRevB.58.14163.

Browning, L. B., H. Y. J. McSween, and M. E. Zolensky (1996), Correlated alteration effects in CM carbonaceous chondrites, *Geochim. Cosmochim. Acta*, *60*, 2621–2633, doi:10.1016/0016-7037(96)00121-4.

Carter-Stiglitz, B., et al. (2001), Unmixing magnetic assemblages and the magnetic behavior of bimodal mixtures, *J. Geophys. Res.*, *106*, 26,397–26,411, doi:10.1029/2001JB000417.

Chen, D.-X., E. Pardo, and A. Sanchez (2006), Fluxmetric and magnetometric demagnetizing factors for cylinders, *J. Magn. Magn. Mater.*, *306*, 135–146, doi:10.1016/j.jmmm.2006.02.235.

Coey, J. M. D., O. Ballet, A. Moukarika, and J. L. Soubeyroux (1981), Magnetic properties of sheet silicates; 1/1 layer minerals, *Phys. Chem. Miner.*, *7*, 141–148, doi:10.1007/BF00308232.

Coey, J. M. D., A. Moukarika, and O. Ballet (1982), Magnetic order in silicate minerals, *J. Appl. Phys.*, *53*, 8320–8325, doi:10.1063/1.330353.

Coey, J. M. D., T. Bakas, C. M. McDonagh, and F. J. Litterst (1989), Electrical and magnetic properties of cronstedtite, *Phys. Chem. Miner.*, *16*, 394–400, doi:10.1007/BF00199561.

Eeckhout, S. G., E. De Grave, A. Lougear, M. Gerdan, C. A. McCammon, A. X. Trautwein, and R. Vochten (2001),

Magnetic properties of synthetic P21/c (Mg-Fe)SiO3 clinopyroxenes as observed from their low-temperature Mössbauer spectra and from SQUID magnetization measurements, *Am. Mineral.*, *86*, 957–964, doi:10.1007/s007100170001.

Elmaleh, A., G. Rousse, B. Devouard, and M. Fialin (2010), Using the magnetic properties of Fe-serpentines for probing early alteration events in CM2 carbonaceous chondrites, Abstract GP43B-1052 presented at 2010 Fall Meeting, AGU, San Francisco, Calif., 13–17 Dec.

Elmaleh, A., S. C. Tarantino, M. Zema, B. Zanda, B. Devouard, and M. Fialin (2011), Low-*T* magnetic properties of 5 CM2 chondrites: Comparison with the signature of cronstedtite and with preliminary results from the Paris chondrite, paper presented at 74th Annual Meeting, Meteorit. Soc., London.

Fiorani, D. (1992), Comparison between fine particles and spin-glass properties, in *Magnetic Properties of Fine Particles*, edited by J.-L. Dormann and D. Fiorani, pp. 135–143, North-Holland, Amsterdam.

Gattacceca, J., P. Rochette, F. Lagroix, P.-E. Mathé, and B. Zanda (2011), Low temperature magnetic transition of chromite in ordinary chondrites, *Geophys. Res. Lett.*, *38*, L10203, doi:10.1029/2011GL047173.

Howard, K. T., G. Benedix, P. A. Bland, and G. Cressey (2009), Modal mineralogy of CM2 chondrites by X-ray diffraction (PSD-XRD). Part 1: Total phyllosilicate abundance and the degree of aqueous alteration, *Geochim. Cosmochim. Acta*, *73*, 4576–4589, doi:10.1016/j.gca.2009.04.038.

Hybler, J., V. Petricek, S. Ďurovič, and L. Smrcok (2000), Refinement of the crystal structure of the cronstedtite-1*T*, *Clays Clay Miner.*, *48*, 331–338, doi:10.1346/CCMN.2000.0480304.

Hybler, J., V. Petricek, J. Fabry, and S. Ďurovič (2002), Refinement of the crystal structure of cronstedtite-2H_2, *Clays Clay Miner.*, *50*, 601–613, doi:10.1346/000986002320679332.

Hyman, M., and M. W. Rowe (1986), Saturation magnetization measurements of carbonaceous chondrites, *Meteoritics*, *21*, 1–22.

Ibers, J. A., and W. C. Hamilton (1974), *International Tables for X-Ray Crystallography*, vol. 4, Kynoch, Birmingham, U. K.

Johnson, C. A., and M. Prinz (1991), Chromite and olivine in Type-Ii chondrules in carbonaceous and ordinary chondrites—Implications for thermal histories and group differences, *Geochim. Cosmochim. Acta*, *55*, 893–904, doi:10.1016/0016-7037(91)90349-A.

Kąkol, Z., and J. M. Honig (1989), The variation of Verwey transition temperature with oxygen stoichiometry in magnetite, *Solid State Commun.*, *70*, 967–969, doi:10.1016/0038-1098(89)90638-8.

Kirschbaum, K., A. Martin, and A. A. Pinkerton (1997), Lambda/2 contamination in charge-coupled-device area-detector data, *J. Appl. Crystallogr.*, *30*, 514–516, doi:10.1107/S0021889897004214.

Klein, F., W. Bach, N. Joens, T. McCollom, B. Moskowitz, and T. Berquo (2009), Iron partitioning and hydrogen generation during serpentinization of abyssal peridotites from 15°N on the Mid-Atlantic Ridge, *Geochim. Cosmochim. Acta*, *73*, 6868–6893, doi:10.1016/j.gca.2009.08.021.

Knop, O., C.-H. Huang, K. I. G. Reid, J. S. Carlow, and F. W. D. Woodhams (1976), Chalkogenides of the transition elements. X-ray, neutron, Mössbauer and magnetic studies of pentlandite and the π phases π(Fe, Co, Ni, S), Co_8MS_8 and $Fe_4Ni_4MS_8$ (M = Ru, Rh, Pd), *J. Solid State Chem.*, *16*, 97–116, doi:10.1016/0022-4596(76)90012-8.

Kogure, T., J. Hybler, and H. Yoshida (2002), Coexistence of two polytypic groups in cronstedtite from Lostwithiel, England, *Clays Clay Miner.*, *50*, 504–513, doi:10.1346/000986002320514226.

Kohout, T., A. Kosterov, M. Jackson, L. J. Pesonen, G. Kletetschka, and M. Lehtinen (2007), Low-temperature magnetic properties of the Neuschwanstein EL6 meteorite, *Earth Planet. Sci. Lett.*, *261*, 143–151, doi:10.1016/j.epsl.2007.06.022.

Lauretta, D. S., X. Hua, and P. R. Buseck (2000), Mineralogy of fine grained rims in the ALH 81002 CM chondrite, *Geochim. Cosmochim. Acta*, *64*, 3263–3273, doi:10.1016/S0016-7037(00)00425-7.

Lindgren, P., M. R. Lee, M. Sofe, and M. J. Burchell (2011), Microstructure of calcite in the CM2 carbonaceous chondrite LON 94101: Implications for deformation history during and/or after aqueous alteration, *Earth Planet. Sci. Lett.*, *306*, 289–298, doi:10.1016/j.epsl.2011.04.022.

Marcaillou, C., M. Muñoz, O. Vidal, T. Parra, and M. Harfouche (2011), Mineralogical evidence for H(2) degassing during serpentinization at 300°C/300 bar, *Earth Planet. Sci. Lett.*, *303*, 281–290, doi:10.1016/j.epsl.2011.01.006.

Mattsson, J., T. Jonsson, P. Nordblad, H. Aruga Katori, and A. Ito (1995), No phase transition in a magnetic field in the Ising spin glass $Fe_{0.5}Mn0_{0.5}TiO_3$, *Phys. Rev. Lett.*, *74*, 4305–4308, doi:10.1103/PhysRevLett.74.4305.

McSween, H. Y. (1979), Alteration in CM carbonaceous chondrites inferred from modal and chemical variations in matrix, *Geochim. Cosmochim. Acta*, *43*, 1761–1770, doi:10.1016/0016-7037(79)90024-3.

Metzler, K., A. Bischoff, and D. Stöffler (1992), Accretionary dust mantles in CM chondrites: Evidence for solar nebula processes, *Geochim. Cosmochim. Acta*, *56*, 2873–2897, doi:10.1016/0016-7037(92)90365-P.

Muxworthy, A. R. (1999), Low-temperature susceptibility and hysteresis of magnetite, *Earth Planet. Sci. Lett.*, *169*, 51–58, doi:10.1016/S0012-821X(99)00067-9.

Muxworthy, A. R., and E. McClelland (2000), Review of the low-temperature magnetic properties of magnetite from a rock magnetic perspective, *Geophys. J. Int.*, *140*, 101–114, doi:10.1046/j.1365-246x.2000.00999.x.

Mydosh, J. A. (1993), *Spin Glasses: An Experimental Introduction*, Taylor and Francis, London.

Néel, L. (1949), Théorie du traînage magnétique des ferromagnétiques en grains fins avec applications aux terres cuites, *Ann. Geophys.*, *5*, 99–136.

Nespolo, M., and G. Ferraris (2001), Effects of the stacking faults on the calculated electron density of mica polytypes—The Ďurovič effect, *Eur. J. Mineral.*, *13*, 1035–1045, doi:10.1127/0935-1221/2001/0013-1035.

Oufi, O., and M. Cannat (2002), Magnetic properties of variably serpentinized abyssal peridotites, *J. Geophys. Res.*, *107*(B5), 2095, doi:10.1029/2001JB000549.

Özdemir, Ö., and D. J. Dunlop (1999), Low-temperature properties of a single crystal of magnetite oriented along principal magnetic axes, *Earth Planet. Sci. Lett.*, *165*, 229–239, doi:10.1016/S0012-821X(98)00269-6.

Palmer, E. E., and D. S. Lauretta (2011), Aqueous alteration of kamacite in CM chondrites, *Meteorit. Planet. Sci.*, *46*, 1587–1607, doi:10.1111/j.1945-5100.2011.01251.x.

Parker, D., V. Dupuis, F. Ladieu, J.-P. Bouchaud, E. Dubois, R. Perzynski, and E. Vincent (2008), Spin-glass behavior in

an interacting γ-Fe2O3 nanoparticle system, *Phys. Rev. B*, *77*, 104428, doi:10.1103/PhysRevB.77.104428.

Pouchou, J. L., and F. Pichoir (1985), "PAP" phi-rho-Z procedure for improved quantitative microanalysis, in *Microbeam Analysis*, edited by J. L. Armstrong, pp. 104–106, San Francisco Press, San Francisco, Calif.

Prozorov, R., T. Prozorov, S. K. Mallapragada, B. Narasimhan, T. J. Williams, and D. A. Bazylinski (2007), Magnetic irreversibility and the Verwey transition in nanocrystalline bacterial magnetite, *Phys. Rev. B*, *76*, 054406, doi:10.1103/PhysRevB.76.054406.

Rancourt, D. G., I. A. D. Christie, G. Lamarche, I. Swainson, and S. Flandrois (1994), Magnetism of synthetic and natural annite mica: Ground state and nature of excitations in an exchange-wise two-dimensional easy-plane ferromagnet with disorder, *J. Magn. Magn. Mater.*, *138*, 31–44, doi:10.1016/0304-8853(94)90396-4.

Rochette, P., G. Fillion, J.-L. Mattéi, and J. Dekkers (1990), Magnetic transition at 30-34 Kelvin in pyrrhotite: Insight into a widespread occurrence of this mineral in rocks, *Earth Planet. Sci. Lett.*, *98*, 319–328, doi:10.1016/0012-821X(90)90034-U.

Rochette, P., et al. (2008), Magnetic classification of stony meteorites: 2. Non-ordinary chondrites, *Meteorit. Planet. Sci.*, *43*, 959–980, doi:10.1111/j.1945-5100.2008.tb01092.x.

Rubin, A. E. (2007), Petrography of refractory inclusions in CM2.6 QUE 97990 and the origin of melilite-free spinel inclusions in CM chondrites, *Meteorit. Planet. Sci.*, *42*, 1711–1726, doi:10.1111/j.1945-5100.2007.tb00532.x.

Rubin, A. E., J. M. Trigo-Rodríguez, H. Huber, and J. T. Wasson (2007), Progressive aqueous alteration of CM carbonaceous chondrites, *Geochim. Cosmochim. Acta*, *71*, 2361–2382, doi:10.1016/j.gca.2007.02.008.

Sheldrick, G. M. (1998), SHELX97—Programs for crystal structure analysis (release 97-2), Inst. für Anorganische Chem. der Univ., Göttingen, Germany.

Sheldrick, G. M. (2004), SADABS: Program for empirical absorption correction of area detector data, Univ. of Göttingen, Göttingen, Germany.

Thorpe, A. N., F. E. Senftle, and J. R. Grant (2002), Magnetic study of magnetite in the Tagish Lake meteorite, *Meteorit. Planet. Sci.*, *37*, 763–771, doi:10.1111/j.1945-5100.2002.tb00853.x.

Tomeoka, K., and P. R. Buseck (1985), Indicators of aqueous alteration in CM carbonaceous chondrites: Microtextures of a layered mineral containing Fe, S, O and Ni, *Geochim. Cosmochim. Acta*, *49*, 2149–2163, doi:10.1016/0016-7037(85)90073-0.

Tomeoka, K., and P. R. Buseck (1988), Matrix mineralogy of the Orgueil CI carbonaceous chondrite, *Geochim. Cosmochim. Acta*, *52*, 1627–1640, doi:10.1016/0016-7037(88)90231-1.

Zanda, B., M. Bourot-Denise, R. H. Hewins, J. A. Barrat, and J. Gattacceca (2010), The Paris CM chondrite yields new insights on the onset of parent body alteration, paper 5312 presented at 73rd Meeting, Meteorit. Soc., New York.

Zega, T. J., and P. R. Buseck (2003), Fine-grained-rim mineralogy of the Cold Bokkeveld CM chondrite, *Geochim. Cosmochim. Acta*, *67*, 1711–1721, doi:10.1016/S0016-7037(02)01172-9.

Zolensky, M. E., R. Barrett, and L. Browning (1993), Mineralogy and composition of matrix and chondrule rims in carbonaceous chondrites, *Earth Planet. Sci. Lett.*, *57*, 3123–3148, doi:10.1016/0016-7037(93)90298-B.

Zolensky, M. E., A. N. Krot, and G. Benedix (2008), Low-temperature alteration in asteroids, *Rev. Mineral. Geochem.*, *68*, 429–462, doi:10.2138/rmg.2008.68.15.